A senescence-specific lncRNA controls metabolic rewiring of senescent cells

Elena Grossi[1,2#], Francesco P. Marchese[1,2], Jovanna González[1,2], Enrique Goñi[1,2], Alicia Amadoz[1,2], Nicolás Herranz[3], Marta Montes[1,2] *, Maite Huarte[1,2] *

[1] Center for Applied Medical Research, University of Navarra, Pamplona, Spain

[2] Institute of Health Research of Navarra (IdiSNA), Pamplona, Spain

[3] Vall d'Hebron Institute of Oncology (VHIO), Barcelona, Spain; Vall d'Hebron Institute of Research (VHIR), Barcelona, Spain

[#] Current address: Department of Oncological Sciences, Icahn School of Medicine at Mount Sinai, New York, NY, USA; Department of Dermatology, Icahn School of Medicine at Mount Sinai, New York, NY, USA.

* Co-corresponding authors: mmontesr@unav.es; maitehuarte@unav.es

ABSTRACT

Despite the classical view of senescence as passive growth arrest, it is an active process with profound implications for cellular homeostasis. Senescent cells remain metabolically active to be able to cope with the energetic demand of the senescence program, although the precise mechanisms underlying this metabolic reprogramming are just beginning to emerge. Here we have identified *sin-lncRNA,* a previously uncharacterized lncRNA, highly specific of senescent cells, and transcriptionally induced by C/EBPβ, the master regulator of the senescence-associated secretory phenotype (SASP). While being strongly activated in senescence, *sin-lncRNA* knockdown reinforces the senescence program by affecting oxidative phosphorylation and mitochondrial function. *sin-lncRNA* interacts with the TCA enzyme dihydrolipoamide S-succinyltransferase (DLST) to facilitate its proper. s*in-lncRNA* depletion increases DLST nuclear

translocation, favoring a metabolic shift from oxidative phosphorylation to a glycolytic phenotype. Moreover, while *sin-lncRNA* expression remains low in highly proliferative cancer cells, it is strongly induced upon cisplatin-induced senescence. Knockdown of *sin-lncRNA* in ovarian cancer cells results in deficient oxygen consumption and increased extracellular acidification, sensitizing the cells to cisplatin treatment. Altogether, these results indicate that *sin-lncRNA* is specifically induced in cellular senescence to maintain metabolic homeostasis. Our findings reveal a new regulatory mechanism in which a lncRNA contributes to the adaptive metabolic changes in senescent cells, unveiling the existence of an RNA-dependent metabolic network specific to senescent cells.

INTRODUCTION

Senescence is a permanent state of growth arrest that can be induced by different types of stress, such as shortening of telomeres due to extensive replication, DNA damage, oxidative stress, chemotherapy treatment or oncogene overexpression [1]. Oncogene-induced senescence (OIS) was firstly described by Serrano *et al*. when they observed that expression of the HRASV12 oncogene in primary fibroblast induced a permanent cell-cycle arrest [2]. Later evidence has shown that OIS is a potent tumor suppressive mechanism that can repress malignant transformation by inducing a coordinated activation of tumor suppressor pathways, such as p53 and p16 [3, 4]. Senescent cells present characteristic morphological and biochemical features such as enlarged size, halted proliferation, activation of senescence-associated (SA) β-galactosidase activity and increased expression of cell cycle inhibitors [1]. Furthermore, in several types of senescence the cells secrete a combination of interleukins, metalloproteases and growth factors, collectively known as the senescence-associated secretory phenotype (SASP) [5-7]. While the SASP reinforces senescence, its chronic activation can have protumorigenic effects and contribute to several aging related pathologies [8]. In fact, the persistence of therapy-induced senescence cancer cells in the tumor has been linked to resistance to chemotherapy [9, 10]. There is therefore a critical need to develop combinatorial approaches to not only stop proliferation, but also induce the elimination of the senescent tumor cells.

Despite their decreased proliferative potential, senescent cells are metabolically active in order to cope with the energetic demands of the senescence program [11]. Indeed, metabolic reprogramming is considered a hallmark of senescence [12]. In general, senescent cells accumulate dysfunctional mitochondria resulting in an increase of reactive oxygen species (ROS) [13-15]. However, different types of senescence can lead to different types of metabolic alterations. For instance, OIS cells display a significant increase in tricarboxylic acid (TCA) cycle intermediates, oxidative phosphorylation (OXPHOS) [16] and mitochondrial fatty acid oxidation [17], while fibroblasts undergoing replicative senescence show increased glycolysis and reduced OXPHOS [18-20]. The fact that different triggers of senescence result in broad metabolic differences indicate that the interplay between senescent cells and metabolism is highly dynamic and context

60 dependent. Yet, the mechanisms underlying this regulatory process remain largely unexplored. In this
61 context, long non-coding RNAs (lncRNAs) represent a relatively uncharted territory for investigation.

62 LncRNAs are transcripts recently defined as longer than 500 nucleotides with exquisite cell-type specific
63 expression patterns that lack protein-coding potential [21]. They are tightly regulated during development or
64 in response to signaling pathways [22]. Although it is still unclear how many of the thousands of annotated
65 lncRNAs have a significant biological effect, several have been found to be essential for the regulation of
66 key cellular processes, such as proliferation and differentiation, as well as a broad range of diseases
67 including cancer [23, 24]. Notably, our previous work and other laboratories' have reported that specific
68 lncRNAs are differentially expressed during senescence induction [25, 26], regulating multiple senescence
69 aspects, from transcriptional response to SASP production [27-30]. Intriguingly, recent studies have involved a
70 number of lncRNAs in the regulation of cellular metabolism [31-34]; and ncRNAs are emerging as regulators of
71 metabolic enzymes [35]. However, the contribution of this plastic class of molecules to the metabolic
72 reprogramming of senescent cells remains unknown.

73 Here we report the identification of the senescence-specific lncRNA, *sin-lncRNA*, which is induced in
74 senescence to prevent uncontrolled metabolic alterations by regulating the function of a key metabolic
75 enzyme. Together, our results provide evidence of an RNA-dependent metabolic network specific of the
76 senescent cellular state.

77 **RESULTS**

78 **Oncogene-induced senescence leads to a broad gene expression response, encompassing alterations**
79 **in lncRNAs**

80 Although the importance of lncRNAs in a variety of cellular processes is now fully recognized, only a
81 handful of lncRNAs have been described as directly implicated in cellular senescence. To identify
82 noncoding regulators of this process, we analyzed RNA-seq data from a cellular system that recapitulates
83 senescence induction *in vitro* thanks to the controlled activation of an oncogene [36]. IMR90 non-
84 immortalized lung fibroblasts were engineered to express an oncogenic HRAS variant ($HRAS^{G12V}$) fused to

85 the estrogen receptor (ER:RAS), which is activated following 4-hydroxy-tamoxifen (4OHT) administration
86 (Figure 1A) [5, 37]. Multiple senescence markers, such as arrest of proliferation, increased expression of pro-
87 inflammatory factors and tumor suppressors along with detectable β-galactosidase staining, were
88 observed, ensuring a proper senescence progression (Suppl. Figure 1A-E). Furthermore, we monitored the
89 chromatin remodeling linked to OIS by analyzing the presence of senescence-associated heterochromatin
90 foci (SAHF) as well as an increase in H3K9me3 and γH2AX foci (Suppl. Figure 1F, G). By mining RNAseq
91 data previously generated in this cell system [36], we detected more than 4720 genes differentially expressed
92 upon induction of senescence (log2FC>1; padj<0.05), including not only many coding genes (3456) but also
93 lncRNAs (951) (Figure 1B and Suppl. Figure 1H). The majority of lncRNAs (62%) were downregulated,
94 which might reflect cell cycle inhibition during senescence, whereas the remaining 38% of lncRNAs were
95 upregulated. We focused our attention on lncRNAs highly induced upon OIS, as we speculated, they might
96 play a direct role in the senescence process, and we verified their upregulation at different time points of
97 OIS progression (Figure 1C and Suppl. Figure 1I).

98 ***sin-lncRNA* is a senescence-specific lncRNA transcriptionally induced by C/EBPβ**

99 Since several lncRNAs increased their expression in OIS, we sought to investigate their possible
100 contribution to this cellular process. Interestingly, we observed a previously uncharacterized lncRNA
101 (*RIPOR3-as1)* as one of the most significantly and strongly upregulated genes, with an induction
102 comparable to that of key senescence genes *CKN2A, CXCL1* and *IL6* (Figure 1B and Suppl. Table 1). We
103 consequently renamed it *senescence-induced lncRNA* or *sin-lncRNA*. *sin-lncRNA* is an intronic lncRNA
104 located in chromosome 20 and transcribed in the antisense orientation of the protein-coding gene *RIPOR3*
105 (Figure 1D, Suppl. Figure 2A, B). This noncoding transcript lacks coding potential (Suppl. Figure 2C) and
106 presents two poly-adenylated isoforms annotated by GENCODE (v41); a longer one (638 nts), composed
107 by three exons, and a shorter one (539 nts) of four exons. However, only the shorter isoform is expressed
108 and highly upregulated upon 4OHT treatment in IMR90 fibroblasts, according to both sequencing data and
109 RT-qPCR performed with different primer sets (Figure 1D and Suppl. Figure 2A). This observation was
110 confirmed by absolute quantification by RT-qPCR, which showed that *sin-lncRNA* is lowly expressed in

111 proliferating conditions with ~9 copies per cell, while, upon senescence induction, the expression of its
112 short isoform increases up to ~86 copies (Suppl. Figure 2D).

113 Interestingly, *sin-lncRNA* levels increased only at later stages of senescence (Figure 1C and Suppl. Figure
114 2A), prompting us to investigate whether *sin-lncRNA* upregulation was dependent on the full activation of
115 a senescence program or it was rather related to the induction of the HRAS oncogene in OIS. To this aim,
116 we analyzed *sin-lncRNA* expression levels in different types of senescence, such as replicative senescence -
117 achieved by prolonged culture of untransformed IMR90 fibroblasts - and senescence induced by ionizing
118 radiation (γ-irradiation). In both cases *sin-lncRNA* expression was strongly induced in the senescent
119 context, correlating with known senescence markers, such as $p16^{INK4a}$ and *IL6* (Figure 1E and Suppl. Figure
120 2E) and independently of HRAS or the approach used.

121 Due to the strong and highly specific *sin-lncRNA* induction in senescence, we speculated that senescence-
122 specific factors might regulate the expression of this lncRNA. We took advantage of publicly available
123 ChIP-seq data generated in IMR90 cells to examine *sin-lncRNA* genomic region, finding that the
124 transcription factor C/EBPβ was bound to several positions in the proximity of *sin-lncRNA* TSS and gene
125 body (Figure 1D). Interestingly, C/EBPβ exerts an important role in the later stages of senescence
126 induction, mainly by activating genes related to inflammation and SASP [38]. After confirming the previously
127 reported C/EBPβ upregulation in OIS [6] (Suppl. Figure 2F), we depleted C/EBPβ in senescent cells and
128 analyzed *sin-lncRNA* expression (Figure 1F, G and Suppl. Figure 2G). Notably, the induction of *sin-lncRNA*
129 in senescence was prevented by C/EBPβ depletion, similarly to what occurred to *IL1β*, *IL6* and *IL8,* other
130 canonical targets of this transcription factor (Figure 1G). To further investigate whether or not *sin-lncRNA*
131 is a C/EBPβ transcriptional target, we performed ChIP-qPCR of this transcription factor in proliferative and
132 senescent conditions (Figure 1H). C/EBPβ was found enriched at *sin-lncRNA* regulatory regions and its
133 binding increased in senescent cells (Figure 1H), supporting the evidences that the senescence driver
134 C/EBPβ controls *sin-lncRNA* expression at later stages of senescence induction and suggesting that the
135 lncRNA might exert a role in this response.

136 ***sin-lncRNA* contributes to the senescent phenotype**

137 To explore the function of *sin-lncRNA*, we depleted it in senescent IMR90 ER:RAS fibroblasts (Figure 2A
138 and Suppl. Figure 3A) and analyzed several senescence markers at 5 days of induction in order to detect
139 intermediate states before the cells enter a fully senescent phenotype [39]. Interestingly, *sin-lncRNA* KD
140 further decreased proliferation of senescent cells (Figure 2B, C and Suppl. Figure 3B), increased the
141 percentage of β-galactosidase positive cells (Figure 2D) and activated the p53 signaling pathway (Figure
142 2E), indicating that *sin-lncRN*A knockdown reinforces the senescent phenotype. Notably, the opposite
143 phenotype was observed when *sin-lncRNA* was overexpressed in senescent cells, alleviating the senescent-
144 mediated growth arrest (Figure 2H-I and Suppl. Figure 3H-I).

145 To corroborate the broader significance of these results, we took advantage of TIG3 hTERT lung
146 fibroblasts engineered to express an inducible and constitutively active portion of the human BRAF
147 oncogene to drive OIS (TIG3 ΔBRAF:ER) [40]. In this cell system, we again observed reduced proliferation and
148 increased β-galactosidase staining upon *sin-lncRNA* downregulation by RNAi (Suppl. Figure 3C-E),
149 indicating that *sin-lncRNA* depletion leads to the same phenotype in different models of cellular
150 senescence and regardless of the type of oncogene expressed. We also generated TIG3 ΔBRAF:ER cell
151 lines stably depleted of *sin-lncRNA* by CRISPR/Cas9 technology. Despite not being able to isolate viable
152 cell clones with *sin-lncRNA* biallelic deletion, we found that the removal of just one allele was sufficient to
153 decrease *sin-lncRNA* expression, leading to a consistent strengthening of the senescence phenotype
154 (Figure 2F-G and Suppl. Figure 3F-G). Altogether, these results suggest a role for *sin-lncRNA* as a negative
155 regulator of senescence induction.

156 **_sin-lncRNA_ depletion is linked to metabolic alterations and increased oxidative stress in senescent**
157 **cells**

158 To investigate which aspect of the complex senescence pathway is influenced by *sin-lncRNA*, we analyzed
159 the global changes in gene expression by RNA-seq of *sin-lncRNA*-depleted ER:RAS fibroblasts upon
160 senescence induction. RNA-seq analysis identified 295 upregulated and 137 downregulated genes upon
161 *sin-lncRNA* depletion (adj. P-value < 0.01; $\log_2$FC > ±1) (Figure 3A and Suppl. Table 2). After validating

162 some of the differentially expressed transcripts by RT-qPCR (Suppl. Figure 4A), we employed Gene Set
163 Enrichment Analysis (GSEA) to determine enriched pathways associated with the observed changes in
164 gene expression. *sin-lncRNA* knockdown led to the significant upregulation of genes associated to
165 epithelial-to-mesenchymal transition (EMT), as well as pathways generally related to response to stress,
166 such as interferon gamma (IFN-γ) response and p53 pathway. Conversely, growth promoting pathways,
167 such as MYC and E2F targets, were reduced upon *sin-lncRNA* knockdown, in line with the observed
168 changes in cell proliferation (Figure 3B and Suppl. Figure 4B). Interestingly, among the most significantly
169 reduced were several metabolic pathways, such as cholesterol homeostasis and fatty acid metabolism, as
170 well as those related to oxidative phosphorylation (Figure 3B-C).

171 The gene expression alterations linked to *sin-lncRNA* depletion pointed to changes in the metabolic state
172 of the cells. Metabolic rearrangements are considered a hallmark of senescence and in particular,
173 alterations in oxidative phosphorylation (OXPHOS) are known to be linked to senescence [16, 41]. In order to
174 analyze metabolic alterations upon *sin-lncRNA* depletion, we measured the oxygen consumption rate
175 (OCR) coupled to ATP production during OXPHOS by Seahorse assay [42]. Compared to control senescent
176 cells, *sin-lncRNA* knockdown led to the reduction of several key parameters of mitochondrial function,
177 such as Maximal Respiration rate, ATP production, Spare Respiratory Capacity and Coupling Efficiency
178 (Figure 3D, Suppl. Figure 4C). Accordingly, we also observed an increment in extracellular acidification rate
179 (ECAR), a reflection of increased glycolysis (Figure 3E).

180 Since alterations in OXPHOS are also linked to increased oxidative stress, we measured intracellular levels
181 of reactive oxygen and nitrogen species (ROS/RNS) and observed a significant enrichment of oxidant
182 species in *sin-lncRNA*-depleted senescent ER:RAS cells (Figure 3F), suggesting that *sin-lncRNA* is involved
183 in the control of oxidative stress in senescent cells. Moreover, since an increase in oxidant species and
184 metabolic dysfunctions can reinforce senescence [43, 44] we hypothesized that *sin-lncRNA* depletion might
185 exacerbate senescence-related mitochondrial alteration and promote oxidative stress, thereby leading to
186 the observed senescence reinforcement. Indeed, blocking ROS accumulation by N-acetyl-L-cysteine

187 (NAC) treatment [45, 46] restored cell growth and reduced SA-β-galactosidase activation in senescent cells
188 depleted for *sin-lncRNA* (Figure 3G and Suppl. Figure 4D). Together these data support the notion that *sin-*
189 *lncRNA* contributes to control the metabolic program and oxidative stress response of senescent cells.

190 **_sin-lncRNA_ interacts with DLST and controls its subcellular localization**

191 LncRNAs have been previously associated with defects in oxidative stress and metabolic pathways, in
192 particular in cancer, where they alter gene programs through different mechanisms [22, 47]. To elucidate how
193 *sin-lncRNA* regulates metabolic response of senescent cells, we first analyzed *sin-lncRNA* subcellular
194 localization by RNA-FISH and cellular fractionation in cells depleted or not of the lncRNA. We found *sin-*
195 *lncRNA* to be mainly enriched in the cytoplasm of senescent fibroblasts (Figure 4A and Suppl. Figure 4E).
196 Therefore, *sin-lncRNA* likely acts in the cytoplasm to control proliferative and metabolic pathways of
197 senescent cells. We then reasoned that *sin-lncRNA* function would be mediated through interacting
198 proteins. We then set out to identify its protein interactors by performing RNA pulldown by incubating *in*
199 *vitro* transcribed *sin-lncRNA* or an unrelated control RNA with senescent IMR90 ER:RAS extracts. We
200 isolated a band of ~50-55 kDa unique for *sin-lncRNA*. Mass spectrometry (MS) analysis revealed several
201 proteins enriched (≥2 unique peptides) specifically associated with sin-lncRNA but not to the control RNA
202 MS (Figure 4B and Suppl. Table 3). Notably, the most abundant proteins retrieved by MS analysis
203 (Dihydrolipoamide S-succinyltransferase (DLST) and DEAD-Box Helicase 28 (DDX28)) have a recognized
204 role in mitochondrial function [48], in line with our findings linking sin-lncRNA to senescent cell metabolism.
205 DLST, identified as the main *sin-lncRNA* interactor, is the E2 component of the α-ketoglutarate (αKG)
206 dehydrogenase complex (KGDH), which is essential for the entry of glutamine into the tricarboxylic acid
207 (TCA) cycle [49] (Figure 4C). We independently confirmed the interaction between the endogenous DLST
208 and *sin-lncRNA* by RNA Immunoprecipitation in senescent fibroblasts (Figure 4D and Suppl. Fig 5B),
209 suggesting that they function coordinately. We therefore sought to investigate whether DLST depletion
210 could reproduce the phenotypic alterations observed upon *sin-lncRNA* knockdown in senescent cells, as
211 previous reports demonstrated increased ROS production upon DLST knockdown [50]. Indeed, DLST
212 knockdown in senescent fibroblasts led to an increase in the percentage of β-galactosidase positive cells

and decreased cell growth (Figure 4E, F and Suppl. Figure 4F), thus phenocopying *sin-lncRNA* knockdown. Moreover, DLST knockdown resulted in similar expression changes of genes affected by *sin-lncRNA* downregulation (Suppl. Figure 4G), suggesting that DLST and the lncRNA control the same cellular pathways. Consistently with the increased ECAR observed in *sin-lncRNA* Knockdown cells (Figure 3E), we observed an increase in lactate secretion in both *sin-lncRNA* and DLST-depleted senescent cells compared to control cells, suggesting a shift to a glycolytic phenotype (Figure 4G).

Altogether, these results show that *sin-lncRNA* is upregulated during senescence to maintain a correct balance in metabolic substrate consumption by regulating DLST engagement.

Our data suggest that *sin-lncRNA*, which physically interacts with DLST, is functionally connected to the enzyme. However, DLST RNA and protein levels were not affected upon *sin-lncRNA* knockdown and remained stable upon senescence induction (Suppl. Figure 4G-I), indicating that neither *sin-lncRNA* nor cellular senescence modulate DLST expression. We then shifted our attention to the subcellular localization of DSLT, which is encoded by a nuclear gene, and typically shuttles between different subcellular compartments. While its main activity takes place in the mitochondria, it is also localized in the cytoplasm and the nucleus of the cell [50-52]. We therefore investigated whether DLST localization might be regulated by the lncRNA. Interestingly, cellular fractionation of senescent cells upon *sin-lncRNA* depletion showed that DLST levels were significantly decreased in the cytoplasm and increased in the nuclear fraction of senescent cells in absence of the lncRNA (Figure 4H). These results suggest that *sin-lncRNA* might have an impact on the metabolic enzyme DLST in senescent cells by modulating its subcellular localization.

sin-lncRNA **regulates OXPHOS in ovarian cancer cells**

Our results indicate that *sin-lncRNA* is a regulator of the metabolic state of the senescent cells. To gain insight into the potential significance of *sin-lncRNA* function in a physio-pathological context, we interrogated gene expression data of tumor samples available through The Cancer Genome Atlas (TCGA) portal. While *sin-lncRNA* presented low expression across cancer types (Suppl. Figure 5A), its expression negatively correlated with that of genes involved in active cell division, such as cyclins, as *CCNA2*, and

members of the origin of replication complex (ORC), such as *ORC1* and *MCM6* [53] (Suppl. Figure 5B). Accordingly, terms related to cell cycle and mitosis were the most enriched Gene Ontology pathways associated with these genes (Suppl. Figure 5C). Since all these cell division-related genes presented a negative correlation with the senescence-specific *sin-lncRNA*, we speculated that a high expression of this noncoding transcript would predict cells with arrested cell cycle (*e.g.* senescent/quiescent cells), in line with the upregulation of *sin-lncRNA* upon OIS.

While tumor cells are highly proliferative, it has been shown that chemotherapy can induce cellular senescence, which can be linked to the resistance to treatment [10]. To investigate the potential significance of *sin-lncRNA* in response to cancer therapy, we analyzed the expression of the lncRNA in cisplatin-treated ovarian cancer cells, given their ability to undergo senescence upon treatment with platinum-based agents [54]. 10 days after cisplatin treatment, COV362 cells displayed a fully senescent phenotype, as confirmed by the expression of senescence markers, such as β-galactosidase and the induction of cell cycle inhibitors and SASP components (Figure 5A-B). Interestingly, we observed a strong increase of *sin-lncRNA* expression in the senescent cells, whereas it was undetectable in untreated cells (Figure 5C). Cisplatin treatment also upregulated C/EBPβ expression (Figure 5D), suggesting that this transcription factor might be responsible for the transcriptional activation of *sin-lncRNA* also in the cancer cells. As previously shown for senescent fibroblasts, knockdown of *sin-lncRNA* in cisplatin-treated COV362 cells reduced the expression of genes involved in OXPHOS pathway (Figure 5E), which was reflected in alterations in the metabolic functions, as a decreased OCR and increased ECAR (Figure 5F, G). Moreover, knockdown of either *sin-lncRNA* or DLST further decreased cell growth compared to control senescent cells (Figure 5H) indicating that depletion of the senescence-specific lncRNA sensitizes ovarian cancer senescent cells to cisplatin treatment.

Altogether, these data provide evidence that a lncRNA uniquely expressed in senescent cells contributes to the configuration of their metabolic state, also when senescence is induced in cancer cells, thus representing a valuable marker and potential target in aging and cancer.

265 **DISCUSSION**

266 Although senescence has been traditionally considered a static terminal condition, it is now recognized as
267 a dynamic stepwise process, which involves a plethora of factors that coordinately ensure its correct
268 progress. We have identified a lncRNA that is specifically expressed at later stages of senescence induction
269 to maintain the metabolic balance of these cells. Such precise induction is linked to a timely transcriptional
270 activation mediated by the SASP (senescence-associated secretory phenotype) master regulator C/EBPβ;
271 a transcription factor known to promote the later inflammatory phase of the senescent program [38].
272 Remarkably, depletion of *sin-lncRNA* is linked to the activation of some inflammatory signals as well as
273 extracellular matrix remodeling pathways, gene networks that are induced during the second phase of
274 senescence induction. *sin-lncRNA* depletion reinforces the senescence response, altering many of the
275 canonical senescence markers. This is likely a consequence of the augmented ROS production, which
276 feeds forward the senescent phenotype.

277 Mitochondria are the main source of ROS in the cell [55]. Interestingly, one of the most deregulated
278 pathways upon *sin-lncRNA* depletion is oxidative phosphorylation (OXPHOS), which reflects mitochondrial
279 dysfunction and results in high levels of ROS production [56]. High levels of ROS are critical for onset and
280 maintenance of cellular senescence, although it remains difficult to decipher whether they are the cause or
281 consequence of the senescence process [57]. Nevertheless, several factors are involved in feedback
282 mechanisms to prevent an uncontrolled ROS increase [58]. We have found that *sin-lncRNA* interacts with
283 DLST, an enzyme of the TCA cycle, a process that is tightly interconnected to OXPHOS and a main source
284 of ROS [59]. Interestingly, it has been previously shown that the KGDH complex is sensitive to ROS and
285 involved in ROS production [60], and inhibition of this enzyme might be critical in the metabolic deficiency
286 induced by oxidative stress [61]. Accordingly, DLST depletion in senescent cells not only mimics *sin-lncRNA*
287 knockdown by exacerbating growth arrest and β-galactosidase staining but also impairs cell metabolism.
288 In fact, both *sin-lncRNA* and DLST downregulation result in increased extracellular acidification rate and

lactate production, suggesting a shift in the energy production pathway towards glycolysis. This may reflect a mechanism for escaping the restrictions caused by the increased oxidative stress.

Where this interaction takes place remain unknow. However, although DLST function in the TCA occurs in the mitochondria, we cannot exclude that DLST interacts with *sin-lncRNA* in the cytoplasm regulating the availability of DLST for the TCA cycle. Of note, we have identified as a potential *sin-lncRNA* interactor DDX28, which plays a role in OXPHOS and is also known to shuttle from the nucleus to the cytoplasm and mitochondria [48]. Therefore, we cannot exclude that *sin-lncRNA* might regulate other aspects of metabolism at the interface between cytoplasm and mitochondria or even other subcellular compartments. Interestingly, TCA enzymes have been found to translocate into the nucleus where they have roles in epigenetic regulation [62-65]. In particular, the KGDH complex which generates succinyl-CoA, has been demonstrated to contribute to histone succinylation affecting expression of cell cycle genes [52] and altering metabolic states [66]. Whether *sin-lncRNA* knockdown affects histone modification to regulate transcription programs remains to be elucidated.

Platinum-based therapies, currently used as the first line of treatment for patients with ovarian cancer, are known to induce senescence in cancer cells [67]. Although therapy-induced senescence (TIS) has been considered a desirable outcome of cancer therapy, the activation of the senescence program has been shown to induce the rewiring of cellular metabolism promoting the pro-tumorigenic and pro-metatastic potential of ovarian cancer cells [68]. Here, we show that *sin-lncRNA* is specifically induced in ovarian cancer cells that undergo senescence and contributes to sustain the metabolic demands to maintain senescence in cancer cells upon drug treatment. Emerging studies link metabolic reprogramming to cancer drug resistance [69]. Indeed, cisplatin-resistant cells exhibit increased fatty acids (FA) uptake, accompanied by decreased glucose uptake and lipogenesis, indicating reprogramming from glucose to FA dependent anabolic and energy metabolism [70]. Importantly, other metabolic processes affected by *sin-lncRNA* depletion in senescent fibroblasts seen at the transcriptional level include fatty-acid metabolism. Depletion of *sin-lncRNA* might sensitize ovarian tumor cells to cisplatin by metabolic reprogramming at different levels.

316 Metabolic enzymes required for the tricarboxylic acid cycle have been shown to affect senescence by
317 regulating p53 [71]. Importantly, advances in the field of RNA interactome capture have demonstrated that
318 the interplay between metabolic enzymes and RNA is broader than previously considered [35, 72]. These
319 studies have revealed the RNA binding capacity of many enzymes, although the precise mechanism or the
320 physiological relevance requires deeper characterization. Emerging evidence indicates that lncRNAs may
321 contribute to cellular processes in order to adapt and coordinate mitochondrial function to adjust their
322 activities to the environmental conditions [34, 73, 74]. We propose that distinct cellular states or stresses that
323 result in metabolic changes involve the function of ncRNAs that contribute to the re-configuration of the
324 cell metabolism. The exquisite specificity of *sin-lncRNA* in senescence highlights its potential role as a
325 therapeutic target. This discovery paves the way for better comprehension of therapy-induced
326 senescence and its associated implications.
327

328 **MATERIALS AND METHODS**

329 **Cell culture, retroviral infection and treatments**

330 IMR90 lung fibroblasts and HEK-293T cells were purchased from ATCC. TIG3 hTERT pMSCV-ER:ΔBRAF
331 lung fibroblasts [40] were kindly provided by Dr. Lund's laboratory (BRIC - Copenhagen, Denmark). All cell
332 lines were cultured in DMEM medium (GIBCO), supplemented with 10% fetal bovine serum (GIBCO) and 1x
333 penicillin/streptomycin (Lonza). Cells were maintained at 37°C in the presence of 5% CO_2 and tested for
334 mycoplasma contamination regularly, using the MycoAlert Mycoplasma Detection Kit (Lonza).
335 To generate OIS cell systems, viruses were first produced in HEK-293T cells transfected with 12µg of either
336 pLNC-ER:RAS or pLNCX (Empty) vectors, 6µg of gag-pol plasmid, 3µg of pVSVG vector and 1µg of pMAX-
337 GFP plasmid (to check transfection efficiency). Transfection reaction was carried out in opti-MEM medium
338 (GIBCO) using Lipofectamine 2000 (Invitrogen), following manufacturer's instructions. 48 hours after
339 transfection, filtered supernatant supplemented with 4µg/ml polybrene (Santa Cruz), was used to
340 transduce low passage IMR90. Cells were selected with Neomycin-G418 (Sigma) at a final concentration of
341 400µg/ml for at least one week.

342 For senescence induction studies, IMR90 ER:RAS or TIG3-hTERT ΔER:BRAF fibroblasts have been treated
343 with 200nM of 4-hydroxy-tamoxifen (4OHT) for three days unless specified otherwise in the text. When
344 longer time courses were needed, medium was replaced on day 3. Only normal fibroblasts cell lines with
345 less than 20-25 passages were used for experiments.
346 COV362 cells were obtained from SIGMA, kindly provided by Dr. Beatriz Tavira (CIMA) and cultured in
347 DMEM medium (GIBCO), supplemented with 10% fetal bovine serum (GIBCO) and 1x
348 penicillin/streptomycin (Lonza). For senescence induction the cells were treated with 10 μM cisplatin for 10
349 days.
350 N-Acetyl-L-cysteine (NAC, SIGMA) was added at 5 mM 1h prior 4-OHT treatment and for the duration of
351 the experiment.

352 **Irradiation**

353 To induce senescence by ionizing radiation, IMR90 cells were γ-irradiated at 5Gy and harvested at the
354 indicated times. Radiation was delivered at 180 cGy/min using a Siemens Oncor Impression Plus linear
355 accelerator equipped with 6MeV X rays.

356 **RNAi and overexpression studies**

357 For siRNA studies, cells were transfected once with a final concentration of 40nM siRNA using
358 Lipofectamine 2000 (Invitrogen) in opti-MEM medium (GIBCO), unless differently stated in the text.
359 Scrambled siRNA (siRNA CTRL in the text) was used as transfection control. All siRNAs employed
360 in this study were designed using BLOCK-iTTM RNAi Designer
361 (https://rnaidesigner.thermofisher.com/rnaiexpress/) and purchased from Sigma, except C/EBPβ
362 siRNA, a kind gift of Dr. Aragón (CIMA - Pamplona, Spain).
363 To induce senescence in transfected cells, transfection medium was replaced after 6 hours with complete
364 medium containing 200nM 4OHT. When a senescence induction longer than 3 days was needed,
365 transfected cells were trypsinized and re-plated to perform multiple analyses in parallel. All siRNAs used in
366 this study are listed in Table 4.

367 To achieve *sin-lncRNA* overexpression, its shorter isoform has been amplified from IMR90 cDNA with
368 specific primers and cloned in pcDNA3.1(+) vector (purchased from Addgene). For overexpression studies,
369 IMR90 ER:RAS cells has been transiently transfected with 500ng of *sin-lncRNA* or empty pcDNA3.1 plasmid
370 using Lipofectamine 2000 (Invitrogen) in opti-MEM medium (GIBCO). Primers employed for cloning are
371 described in Table 4.

372 **CRISPR-Cas9 gene editing and CRISPR clonal cell lines generation**

373 The CRISPR Design Tool from the Zhang Lab (http://crispr.mit.edu/) was used to find suitable target sites
374 for the Streptococcus pyogenes Cas9 (SpCas9) in *sin-lncRNA* genomic region. Specific guide RNAs
375 (sgRNA_up and sgRNA_dw, see Table 1) were cloned into the lentiviral plasmid lentiCRISPRv2 carrying
376 spCas9 gene and puromycin resistance, a kind gift from Dr. Agami's lab (NKI - Amsterdam, Netherlands)
377 and originally generated in Dr. Zhang's lab [282] (for details, see plasmid reference #5296113 on Addgene
378 website).
379 LentiCRISPR vectors carrying the two independent sgRNAs were separately transfected in HEK-293T cells
380 to generate viral particles, as described above. LentiCRISPR viruses were mixed (ratio 1:1) and used to
381 transduce TIG3-hTERT ΔER:BRAF fibroblasts, then selected with 1µg/ml of puromycin. Single puromycin-
382 resistant TIG3 cells were sorted in 96-well plates, using untreated TIG3 fibroblasts as feeder cells, which
383 were then eliminated by a second round of puromycin selection (0.5µg/ml). Genomic DNA was isolated
384 from puromycin-resistant clones using QuickExtract DNA extraction solution (Lucigen), PCR amplified and
385 tested on agarose gel for accurate deletion.

386 **Cell proliferation assays**

387 For crystal violet assay upon OIS, 1-2×10^4 untreated or transfected cells were plated in 6-well plates and
388 senescence induction was prolonged for 5 days in 4-OHT medium. Cells were fixed with 0.5%
389 glutaraldehyde for 15 min and stained with 0.1% Crystal Violet solution (Sigma) for 30 min. To quantify cell
390 density, cells were incubated with 500µl of 10% acetic acid (Sigma) and collected in ELISA plates.
391 Absorbance was measured by spectrophotometry at 570 nm in a SPECTROstar Nano equipment.
392 For BrdU incorporation assay, cells were labeled with 50 µM BrdU solution (BD Pharmingen) for 16-18

393 hours. In case of senescent cells, OIS was previously induced for 5 days before starting BrdU assay. Then,
394 cells were harvested by trypsinization and BrdU staining was performed using BrdU Flow Kits (BD
395 Pharmingen), according to manufacturer's instructions. Amount of BrdU incorporation was measured by
396 flow cytometry using a FACSCalibur Cell Analyzer (BD Bioscience).

397 **Senescence Associated galactosidase (SA-β-gal) staining**

398 To detect SA-β-gal activity, 1×10^3 of untreated or transfected cells were plated in 6-well plates and
399 senescence was induced for 8 days upon 4-OHT treatment. Cells were fixed with 0.5% glutaraldehyde
400 solution for 15 min at RT and washed with PBS containing 1mM $MgCl_2$ (pH 6.0). Then, cells were incubated
401 overnight at 37°C in X-gal staining solution (1mg/ml X-gal [Thermo Fisher], 0.12 mM $K_3Fe(CN)_6$ [Merk],
402 0.12 mM $K_4Fe(CN)_6$ [Merk], PBS/$MgCl_2$ [pH 6.0]). Cells were washed and percentage of blue cells was
403 counted manually using an inverted microscope.

404 **ROS/RNS measurement assay**

405 Senescent IMR90 ER:RAS fibroblasts transfected with *sin-lncRNA* targeting or control siRNAs were
406 collected by trypsinization and re-suspended at $0.5\text{-}1\times10^6$ cells/ml in Hypotonic Buffer (10mM Tris HCl [pH
407 7.5], 10mM NaCl, 1.5mM $MgCl_2$). To facilitate membrane lysis, cells were incubated for 10 min at 4°C and
408 sonicated for 5 cycles (30''ON-30''OFF) in a Bioruptor sonication device. Cell extract was cleared by
409 centrifugation and assayed for ROS/RNS accumulation by fluorescence-based approach using OxiSelect in
410 vitro ROS/RNS Assay Kit (Cell Biolabs), following manufacturer's instructions. The amount of fluorescent
411 oxidized probe (2', 7' -dichlorodihydrofluorescein or DCF) was measured with a fluorescence plate reader
412 at 480nm excitation / 530nM emission. Data were interpolated to a DCF standard curve to obtain absolute
413 values.

414 **Measurement of oxygen consumption and extracellular acidification**

415 Cellular OCR was measured using a Seahorse XF Cell Mito Stress Test and a Seahorse Bioanalyzer XFe96
416 (Agilent Technologies) according to the manufacturer's standard protocol. Briefly, 200,000 IMR90 cells
417 were reverse transfected with the corresponding siRNAs in 6 well plates. After 24h cells were treated with

418 500 nM 4-OHT. After 3 days of treatment, cells were trypsinized and seeded on Seahorse XF96 Cell Culture
419 microplates to confluence (10000 cells/well) and were subjected to metabolic profiling the next day. For
420 Mito stress tests, cells were cultured for 1 h in a CO_2-free incubator at 37 °C. Oxygen consumption rates
421 (OCR) were monitored at basal conditions and, after sequential injections of 1 µM oligomycin to block the
422 mitochondrial ATP synthase, 1.5 µM FCCP to uncouple oxidative phosphorylation, 1 µM antimycin A and
423 1 µM rotenone were used to fully inhibit mitochondrial respiration and 50 mM 2-deoxygluocse (2-dG) to
424 block glycolysis. Two separate measurements of OCR and extracellular acidification rate (ECAR) from 4
425 independent experiments were taken after the addition of each inhibitor. Samples were normalized based
426 on the protein concentration. All reagents were purchased from Agilent Technologies.

427 **Lactate measurements**

428 IMR90 ER:RAS fibroblasts were transfected with *sin-lncRNA* targeting or control siRNAs and treated with
429 4-OHT for 6 days. The supernatant was harvested and centrifuged for 5 min at 500 g. Lactate levels were
430 measured using Cobas C311 Analyzer with LACT2 kits (Roche Diagnostics GmbH). Human Precinorm y
431 Precipath were used as controls.

432 **Liquid Chromatographic -Mass Spectrometry (LC-MS) metabolomics**

433 *Isotope labelling*

434 6-days senescent IMR90 ER:RAS fibroblasts transfected with siRNA control or siRNA against *sin-lncRNA* or
435 DLST were incubated with glutamine-free DMEM supplemented with 4mM L-$^{13}C_5$-Glutamine (Cambridge
436 Isotopes Laboratories) . After 6 hours the cells were washed with PBS 1x and snap-freeze in liquid nitrogen.
437

438 *Sample preparation and LC/MS methods*

439 LCMS was performed at the Metabolomics Platform at CIC bioGUNE (Donostia, Spain). Cells from three
440 wells (1E6 cells/well) were pooled to obtain one LCMS sample. Therefore, cells were extracted with 200 µL
441 icecold extraction liquid per well. The volume from one well was transferred to the next and finally the
442 resulting 600 µL volume was passed over the three wells two times. The extraction liquid consisted of a
443 mixture of ice-cold methanol/water (50/50 %v/v). Subsequently 400 µL of the cell homogenate plus 400µL

444 of chloroform was transferred to a new aliquot and shaken at 1400 rpm for 60 minutes at 4 °C. Next the
445 aliquots were centrifuged for 30 minutes at 14000 rpm at 4 °C. 250µL of the aqueous phase was
446 transferred to a fresh aliquot. The chilled supernatants were evaporated with a speedvac in approximately
447 2h. The resulting pellets were resuspended in 150 µL water/MeOH (75/25 %v/v). Samples were measured
448 with a UPLC system (Acquity, Waters Inc., Manchester, UK) coupled to a Time-of-Flight mass
449 spectrometer (ToF MS, SYNAPT G2S, Waters Inc.). A 2.1 x 100 mm, 1.7 µm Phenyl-Hexyl column (Waters
450 Inc.), thermostated at 40 °C, was used to separate the analytes before entering the MS. Mobile phase
451 solvent A (aqueous phase) consisted of 99.5% water and 0.5% FA while solvent B (organic phase) consisted
452 of 99.5% MeCN and 0.5% FA. In order to obtain a good separation of the analytes the following gradient
453 was used: from 98% A to 0% A in 2 minutes in curved gradient (#8, as defined by Waters), constant at 0%
454 A for 1 minute, back to 98% A in 0.2 minutes. The flow rate was 0.250 mL/min and the injection volume
455 was 3 µL. After every 6 injections, a sample was injected. The MS was operated in negative electrospray
456 ionization in full scan mode. The cone voltage was 10 V, cone offset was 50V and capillary voltage was 400
457 V. Source temperature was set to 120 °C and capillary temperature to 500 °C. The flow of the cone,
458 desolvation and nebulizer gas (nitrogen) were set to 5 L/h, 6 L/h and 850 L/h, respectively. A 2 ng/mL
459 leucine-enkephalin solution in water/acetonitrile/formic acid (49.9/50/0.1 %v/v/v) was infused at 10 µL/min
460 and used for a lock mass which was measured each 36 seconds for 0.5 seconds. Spectral peaks were
461 automatically corrected for deviations in the lock mass. Extracted ion traces for relevant analytes were
462 obtained in a 10 mDa window in their expected *m/z*-channels. These traces were subsequently smoothed
463 and peak areas integrated with TargetLynx software. Signals of labeled analytes were corrected for
464 naturally occurring isotopes. Since we also had unlabeled experiments, for some metabolites we could
465 determine the naturally occurring isotope-distribution empirically. This was necessary for the first and
466 second isotopomers since correcting with theoretical values did not eliminate these isotopes from
467 unlabeled experiments. This is probably because signals are non-linear with respect to ion-counts, *i.e.*
468 higher ion-counts tend to have *relatively* lower signals than lower ion-counts due to saturation of the
469 detector. The calculated raw signals were adjusted by median fold-change (MFC) adjustment. This is a

470 robust adjustment factor for global variations in signal due to e.g. difference in tissue amounts, signal drift
471 or evaporation. The MFC is based on the total amount of detected mass spectrometric features (unique
472 retention time/mass pairs). The calculations and performance of the MFC adjustment factors are described
473 in the following publications [75, 76].

474 **Immunofluorescence and RNA fluorescence in situ hybridization (RNA-FISH)**

475 For fluorescence-based studies, IMR90 ER:RAS cells were collected by trypsinization after required
476 treatments (as specified in the text) and re-plated on top of cover glasses placed on clean 6-well plates.
477 The following day, cells were washed and fixed for 15 min at room temperature (RT) using 3% methanol-
478 free formaldehyde solution (Thermo Fisher).
479 For immunofluorescence studies, fixed cells were washed (PBS/0.5% NP-40) and incubated first with block
480 solution (10% FBS in wash buffer) for 20 min and then with primary antibody diluted in block solution for 1
481 hour at RT. Antibody solution was washed out and cells were incubated with fluorophore-conjugated
482 secondary antibody for 30 min. After extensive washes, cover glasses were mounted on microscope slides
483 using DAPI-containing mounting solution (Palex Medicals) and pictures were collected with an automated
484 optical microscope running Zen 2 core imaging software (Zeiss), according to standard procedures.
485 For RNA-ISH studies, fluorescein-labeled Locked Nucleic Acid (LNA) DNA probes were designed and
486 synthesized by Exiqon and were hybridized according to manufacturer's protocol with some modifications.
487 Briefly, fixed cells were first incubated with 70% ethanol for 1 hour and then with Acetylation Buffer (0.1M
488 Triethanol Amine, 0.5% (v/v) Acetic Anhydride) for 30 min at RT. To avoid non-specific probe binding, cells
489 were incubated with Hybridization buffer (10% dextran sulfate, 50% formamide, 2x saline-sodium citrate
490 [SSC] buffer) for 1 hour at 55°C. Specific LNA probes were denatured at 92°C for 4 min and then mixed
491 with Hybridization buffer at a final concentration of 20nM. Hybridization was carried out overnight at
492 55°C. The following day, probes residues were eliminated using 2x SSC wash buffer and fixed cells were
493 treated with 3% Hydrogen Peroxide for 30 min at RT. For fluorescein (FAM) detection, cells were first
494 incubated 1 hour with Blocking Buffer (10% heat-inactivated Goat Serum, 0.5% Blocking Reagent [Roche]
495 in PBS-0.5% Tween) and then 1 hour with 1.5U/ml αFAM-POD antibody (Roche) diluted in Blocking Buffer.

After extensive washes, fluorescent signal was developed by 10 min incubation with TSA-Cy3 solution (Perkin Elmer). Residues were eliminated through stringent 4x SSC washing and slides were prepared for microscope detection using DAPI mounting solution, as mentioned above.

Slides were imaged on a fluorescence inverted microscope using a 63x objective. At least 10 optical stacks were acquired per image for DAPI (nuclear stain) and for the fluorescence channel corresponding to the RNA FISH probe (Cy3). Image processing was performed using Zen software (version 2.3 - Zeiss) and for each condition, signal was adjusted on a sample incubated with no probes and used as control for background detection. ImageJ software was employed for stacks deconvolution.

Protein extraction and immunoblot analysis

Cells were lysed for 15 min in rotation at 4 °C using RIPA buffer (150mM NaCl, 25mM Tris HCl [pH 7.5], 2mM EDTA, 0.1% sodium deoxycholate [Na-DOC], 0.1% SDS, 1% Triton X-100) supplemented with 1x cOmplete Protease Inhibitor Cocktail [Roche]. For detection of phosphoproteins, 1x PhosSTOP phosphatase inhibitor [Roche] was freshly added to RIPA solution. Lysed cells were centrifuged at max speed for 10 min at 4 °C and the insoluble pellet was discarded. Protein concentration was estimated by Pierce BCA Protein Assay Kit, using BSA curve as reference and according to manufacturer's instructions. Proteins were separated on denaturing SDS-PAGE gels and transferred to a nitrocellulose membrane [Biorad] following standard procedures. Membranes were blocked using skim milk or BSA (VWR) and probed first for primary and then for HRP-conjugated secondary antibody. Western Lightening ECL- Plus (Perkin Elmer) was employed for chemiluminescence detection of proteins. The list of antibodies used in this study can be found in Table 4.

Cellular Fractionation

IMR90 cells were reverse transfected with control or siRNA 1/3 *sin-lncRNA*. The day after transfection cells were treated with 500 nM 4-OHT for 5 days. Cells were scrapped in cold PBS and centrifuge 5 min 0.2g. Pellets were resuspended in NIB buffer (1.28 M Sucrose, 40 mM Tris pH 7.4, 20 mM $MgCl_2$, 4% Triton X-100), incubated on ice for 20 min and centrifuged 15 min at 2500rpm. The supernatant was kept as the

522 cytosolic fraction and further cleaned by an extra centrifugation step. Nuclear pellets were washed twice
523 with NWB (40 mM Tris pH 7.4, 20 mM $MgCl_2$) by centrifugation 15 min at 2500 rpm. RIPA (150 mM NaCL,
524 25 mM Tris pH 8, 0.1% SDS, 0.1 % Na-Deoxycholate, 2 mM EDTA, 1% Triton X-100) buffer was used to lyse
525 the nuclei. After 10 min centrifugation at max speed the supernatant was isolated as the nuclear fraction.
526 Immunoblot analysis was performed as described above.

527 **Native RNA immunoprecipitation**

528 20×10^6 cells were collected in cold PBS by scraping and lysed in RIP buffer (25 mM Tris-HCl pH 7.4,
529 150 mM KCl, 5mM EDTA, 0.5% Nonidet P-40, 20 U ml^{-1} RNAsin (Promega), 0,5 mM dithiothreitol (DTT)
530 and 1× protease inhibitor mixture Complete (Roche)). After centrifugation, the samples were precleared
531 with Dynabeads Protein A (Invitrogen) for 1 h. One per cent of the sample was used as the input control
532 and the remaining extracts were incubated with 10 µg DLST antibody (Bethyl) or IgG at 4 °C overnight.
533 RNA–antibody complexes were collected by incubation with Dynabeads Protein A. After extensive
534 washing, 1/5 of the sample was used for western blotting control and the remaining for RNA extraction and
535 qRT–PCR analysis, as described below.
536

537 ***In vitro* RNA pulldown**

538 RNA pulldown was performed according to [77]. Briefly, biotin-labeled *sin-lncRNA* and control RNA (cloned in
539 a pcDNA3.1(+) plasmid) were generated in vitro using T7 or T3 RNA polymerase, respectively (Applied
540 Biosystems). Biotinylated RNAs were treated with RNase-free DNase I (Promega), purified on G-50
541 MicroSpin columns (GE Healthcare) and heated to 65C for 10 min and cooled down slowly to 4C to allow
542 proper RNA folding. 10×106 IMR90 ER:RAS were collected after 6 days of senescence induction and total
543 protein extracts were prepared. Cell extracts were then incubated with 10µg of biotinylated RNA in Buffer
544 A (150mM KCl, 25mM Tris pH 7.4, 5mM EDTA, 0.5mM DTT, 0.5% NP40) supplemented with fresh protease
545 inhibitors and yeast tRNA (0.1µg/ml) and rotated overnight at 4C. Dynabeads MyOne Streptavidin T1
546 beads (Invitrogen) were used to isolate RNA-protein complexes. Beads were washed and boiled in 2X

547 Laemmli loading buffer, and retrieved proteins were loaded in a NuPAGE 4%–12% bis-Tris gel (Invitrogen).
548 Gel was stained with the SilverQuest Silver Staining Kit (Thermo Fisher) to identify differential bands
549 comparing *sin-lncRNA* and control RNA samples. Unique bands were cut and submitted for Mass
550 Spectrometry (MS) analysis to the Taplin MS Facility (Harvard University).

551 **Chromatin Immunoprecipitation (ChIP)**

552 C/EBPβ ChIP RT-qPCR was performed as previously described [78]. Briefly, 10×10^6 cells were crosslinked with
553 1% formaldehyde for 10 minutes at RT and nuclei were isolated with cell lysis buffer (5mM Tris pH8.0,
554 85mM KCl, 0.5% NP40, supplemented with fresh 0,5 mM DTT and 1× protease inhibitor mixture Complete
555 (Roche)). Nuclear pellet was then resuspended in RIPA buffer (1X PBS, 1% NP40, 0.5% Na-deoxycholate,
556 0.1% SDS, supplemented with 1× protease inhibitor mixture Complete (Roche)) and chromatin was
557 sheared to a range of 200-500bp by using a Bioruptor instrument (Diagenode) with the following settings:
558 8 cycles LOW, 30"ON/30"OFF. Sonicated chromatin was incubated overnight with 6μg of C/EBPβ or IgG
559 antibody (listed in Table 1) followed by 2h incubation with Dynabeads Protein G beads (Invitrogen). After
560 five washes with LiCl buffer (100mM Tris pH 7.5, 500mM LiCl, 1% NP40, 1% Na-deoxycholate) and TE
561 buffer, DNA was reverse crosslinked by incubating beads in Elution buffer (1% SDS, 0.1M $NaHCO_3$ and
562 Proteinase K (NEB)). C/EBPβ binding was analyzed by qPCR using specific primers (see Table 4).

563 **RNA extraction and RT-qPCR analysis**

564 Total RNA was isolated using TRI reagent (Sigma), treated with DNase I (Invitrogen) and reverse-
565 transcribed using the High-Capacity cDNA Reverse Transcription Kit (Applied Biosystem) with random
566 hexamer primers following manufacturer's instructions. The obtained cDNA was analyzed by quantitative
567 PCR using iTaq Universal SYBR Green supermix (Bio-Rad) in a ViiATM 7 Real-Time PCR System machine
568 (Thermo-Fisher). All reactions were performed in triplicate or quadruplicate and HPRT1 (Hypoxanthine
569 Phosphoribosyl transferase 1) RNA levels were used for normalization, unless specified otherwise in figure
570 legend.
571 To calculate the number of *sin-lncRNA* molecules per cell, *sin-lncRNA* cloned in pcDNA3.1 vector was in
572 vitro transcribed, quantified and converted to number of copies based on its predicted molecular weight.

573 Dilutions of this transcript were retro-transcribed and used as standard curve for qPCR analysis along with
574 cDNA obtained from a precise number of IMR90 proliferating or senescent cells. All qPCR primer
575 sequences are provided in Table 4.

576 **RNA sequencing and data analysis**

577 Raw data of Poly-A+ RNA-seq from proliferating and senescent IMR90 fibroblasts were kindly provided by
578 Dr. Gil's laboratory (Imperial College London, UK) before their publication and are now available at the
579 Gene Expression Omnibus under the accession number GSE61130 [36]. For RNA-seq of IMR90 ER:RAS
580 fibroblasts treated with sin-lncRNA or control siRNA, cells were transfected and 4OHT-treated for 3 days,
581 as described above. Total RNA from samples prepared in biological triplicate was isolated with TRI
582 reagent, purified and treated with DNAse I using RNAeasy mini Kit (Qiagen). After quality evaluation by
583 Experion kit and quantification by Qubit, 1µg of RNA was used for library preparation and sequenced on
584 Illumina HiSeq 2000 (33×10^6 reads per sample, 50bp single-end sequencing modality). Sequenced reads
585 from three different replicates were aligned to hg19 genome using the BOWTIE2 algorithm (v.2.1.0) was
586 used to quantify the number of reads in annotated genes [79, 80] To identify enriched molecular pathways
587 associated with differences in gene expression, Gene Set Enrichment Analysis (GSEA, Broad Institute,
588 http://www.broadinstitute.org/gsea/index.jsp) was performed using the Hallmark gene sets in the Human
589 MSigDB database [81]. Enriched pathways were selected with Normalized Enrichment Score (NES) >±1 and
590 adj.Pvalue<$1e^{-4}$.

591 ***Sin-lncRNA* expression analysis in tumor samples**

592 TCGA RNA-seq expression data was retrieved using R bioconductor library TCGAbiolinks, and represented
593 using R.

594 **Statistical analysis**

595 Unless specified otherwise, experimental data were represented as mean ± standard deviation of at least
596 three biological replicates (unless otherwise stated in figure legends) and significance was determined by

two-tailed unpaired or Student's t-test or one sample using GraphPad software. Significant P values were summarized as follows: not significant (ns); p-value<0.05 (*); p- value<0.01 (**); p-value<0.001 (***).

DATA AVAILABILITY

RNA-seq from proliferating and senescent IMR90 fibroblasts were retrieved from public data (GSE61130) [36]. RNA-seq of *sin-lncRNA* KD and control senescent cells have been deposited in NCBI's Gene Expression Omnibus and are accessible through Gene Expression Omnibus (GEO) [82] repository under the accession number GSE241620 (https://www.ncbi.nlm.nih.gov/geo/query/acc.cgi?acc=GSE241620) with the reviewers token mvylowqmjtotnwx. The mass spectrometry data have been deposited to the ProteomeXchange Consortium via the PRIDE [83] partner repository with the dataset identifier PXD044718 (Username: reviewer_pxd044718@ebi.ac.uk, Password: 8egDSySE).

ACKNOWLEDGEMENTS

We thank Eva Santamaría for her input and help with the seahorse experiments. We thank Beatriz Tavira (CIMA, Universidad de Navarra) for providing the COD362 cells. We thank Lorea Válcarcel (UPV) and Arkaitz Carracerdo (CIC bioGUNE) for their input on the metabolic experiments and Sebastiaan Martijn Van Liempd (Metabolomic Platform, CIC bioGUNE) for his interpretation of the metabolomics results. We thank Victor Segura and Eli Guruceaga, for the guilt-by-association analysis. We thank Jesus Gil (MRC, London) for his input. We acknowledge the ENCODE project and The Cancer Genome Atlas database for their valuable data sets. We thank the rest of the Huarte lab for contributing with helpful discussions. The work was supported by Fondo Europeo de Desarrollo Regional/Ministerio de Ciencia, Innovación y Universidades-Agencia Estatal de Investigación grant (BFU2017–82773-P), European Research Council Consolidator grant (771425) and Worldwide Cancer Research grant (20-0204) and FP7-PEOPLE-2013-ITN. M.M is funded by a MSCA fellowship (HORIZON-MSCA- 2021-PF-01: 101066499).

AUTHORS CONTRIBUTION

623 M.H. and E.G. conceived the study. E.G, M.M and M.H. designed the experiments, analyzed the data and
624 wrote the manuscript with the comments of co-authors. E.G., F.M., J.G. and M.M. performed the
625 experiments. E. G, E. Goñi and A.A. performed bioinformatic analyses. L.B. provided interpretation of the
626 metabolomics experiment. N.H. contributed to the original set-up of the project.
627

628 **COMPETING INTEREST**

629 The authors declare no competing interest.

630 **REFERENCES**

631 1. Kuilman, T., Michaloglou, C., Mooi, W.J. & Peeper, D.S. The essence of senescence. *Genes &*
632 *development* **24**, 2463-2479 (2010).
633 2. Serrano, M., Lin, A.W., McCurrach, M.E., Beach, D. & Lowe, S.W. Oncogenic ras provokes premature
634 cell senescence associated with accumulation of p53 and p16INK4a. *Cell* **88**, 593-602 (1997).
635 3. Michaloglou, C. *et al.* BRAFE600-associated senescence-like cell cycle arrest of human naevi. *Nature*
636 **436**, 720-724 (2005).
637 4. Braig, M. *et al.* Oncogene-induced senescence as an initial barrier in lymphoma development.
638 *Nature* **436**, 660-665 (2005).
639 5. Acosta, J.C. *et al.* Chemokine signaling via the CXCR2 receptor reinforces senescence. *Cell* **133**,
640 1006-1018 (2008).
641 6. Kuilman, T. *et al.* Oncogene-induced senescence relayed by an interleukin-dependent inflammatory
642 network. *Cell* **133**, 1019-1031 (2008).
643 7. Coppe, J.P. *et al.* Senescence-associated secretory phenotypes reveal cell-nonautonomous
644 functions of oncogenic RAS and the p53 tumor suppressor. *PLoS biology* **6**, 2853-2868 (2008).
645 8. Coppe, J.P., Desprez, P.Y., Krtolica, A. & Campisi, J. The senescence-associated secretory
646 phenotype: the dark side of tumor suppression. *Annu Rev Pathol* **5**, 99-118 (2010).
647 9. Nardella, C., Clohessy, J.G., Alimonti, A. & Pandolfi, P.P. Pro-senescence therapy for cancer
648 treatment. *Nat Rev Cancer* **11**, 503-511 (2011).
649 10. Milanovic, M. *et al.* Senescence-associated reprogramming promotes cancer stemness. *Nature* **553**,
650 96-100 (2018).
651 11. Dorr, J.R. *et al.* Synthetic lethal metabolic targeting of cellular senescence in cancer therapy. *Nature*
652 **501**, 421-425 (2013).
653 12. Gonzalez-Gualda, E., Baker, A.G., Fruk, L. & Munoz-Espin, D. A guide to assessing cellular
654 senescence in vitro and in vivo. *FEBS J* **288**, 56-80 (2021).
655 13. Kwon, S.M., Hong, S.M., Lee, Y.K., Min, S. & Yoon, G. Metabolic features and regulation in cell
656 senescence. *BMB Rep* **52**, 5-12 (2019).
657 14. Lee, A.C. *et al.* Ras proteins induce senescence by altering the intracellular levels of reactive oxygen
658 species. *The Journal of biological chemistry* **274**, 7936-7940 (1999).
659 15. Moiseeva, O., Bourdeau, V., Roux, A., Deschenes-Simard, X. & Ferbeyre, G. Mitochondrial
660 dysfunction contributes to oncogene-induced senescence. *Mol Cell Biol* **29**, 4495-4507 (2009).
661 16. Kaplon, J. *et al.* A key role for mitochondrial gatekeeper pyruvate dehydrogenase in oncogene-
662 induced senescence. *Nature* **498**, 109-112 (2013).
663 17. Quijano, C. *et al.* Oncogene-induced senescence results in marked metabolic and bioenergetic
664 alterations. *Cell Cycle* **11**, 1383-1392 (2012).

665 18. Bittles, A.H. & Harper, N. Increased glycolysis in ageing cultured human diploid fibroblasts. *Biosci*
666 *Rep* **4**, 751-756 (1984).
667 19. James, E.L. *et al.* Senescent human fibroblasts show increased glycolysis and redox homeostasis
668 with extracellular metabolomes that overlap with those of irreparable DNA damage, aging, and
669 disease. *J Proteome Res* **14**, 1854-1871 (2015).
670 20. Kondoh, H. *et al.* Glycolytic enzymes can modulate cellular life span. *Cancer Res* **65**, 177-185 (2005).
671 21. Mattick, J.S. *et al.* Long non-coding RNAs: definitions, functions, challenges and recommendations.
672 *Nat Rev Mol Cell Biol* **24**, 430-447 (2023).
673 22. Statello, L., Guo, C.J., Chen, L.L. & Huarte, M. Gene regulation by long non-coding RNAs and its
674 biological functions. *Nat Rev Mol Cell Biol* **22**, 96-118 (2021).
675 23. Qureshi, I.A. & Mehler, M.F. Emerging roles of non-coding RNAs in brain evolution, development,
676 plasticity and disease. *Nat Rev Neurosci* **13**, 528-541 (2012).
677 24. Huarte, M. The emerging role of lncRNAs in cancer. *Nat Med* **21**, 1253-1261 (2015).
678 25. Abdelmohsen, K. *et al.* Senescence-associated lncRNAs: senescence-associated long noncoding
679 RNAs. *Aging cell* **12**, 890-900 (2013).
680 26. Montes, M. *et al.* The lncRNA MIR31HG regulates p16(INK4A) expression to modulate senescence.
681 *Nat Commun* **6**, 6967 (2015).
682 27. Montes, M. & Lund, A.H. Emerging roles of lncRNAs in senescence. *FEBS J* (2016).
683 28. Montes, M. *et al.* The long non-coding RNA MIR31HG regulates the senescence associated
684 secretory phenotype. *Nat Commun* **12**, 2459 (2021).
685 29. Puvvula, P.K. *et al.* Long noncoding RNA PANDA and scaffold-attachment-factor SAFA control
686 senescence entry and exit. *Nat Commun* **5**, 5323 (2014).
687 30. Grossi, E. *et al.* A lncRNA-SWI/SNF complex crosstalk controls transcriptional activation at specific
688 promoter regions. *Nat Commun* **11**, 936 (2020).
689 31. Zhu, Y. *et al.* The long noncoding RNA glycoLINC assembles a lower glycolytic metabolon to
690 promote glycolysis. *Mol Cell* **82**, 542-554 e546 (2022).
691 32. Wang, P., Xu, J., Wang, Y. & Cao, X. An interferon-independent lncRNA promotes viral replication by
692 modulating cellular metabolism. *Science* **358**, 1051-1055 (2017).
693 33. Gandhi, M. *et al.* The lncRNA lincNMR regulates nucleotide metabolism via a YBX1 - RRM2 axis in
694 cancer. *Nat Commun* **11**, 3214 (2020).
695 34. Ding, C. *et al.* A T(reg)-specific long noncoding RNA maintains immune-metabolic homeostasis in
696 aging liver. *Nat Aging* **3**, 813-828 (2023).
697 35. Castello, A., Hentze, M.W. & Preiss, T. Metabolic Enzymes Enjoying New Partnerships as RNA-
698 Binding Proteins. *Trends Endocrinol Metab* **26**, 746-757 (2015).
699 36. Herranz, N. *et al.* mTOR regulates MAPKAPK2 translation to control the senescence-associated
700 secretory phenotype. *Nat Cell Biol* **17**, 1205-1217 (2015).
701 37. Vater, C.A., Bartle, L.M., Dionne, C.A., Littlewood, T.D. & Goldmacher, V.S. Induction of apoptosis by
702 tamoxifen-activation of a p53-estrogen receptor fusion protein expressed in E1A and T24 H-ras
703 transformed p53-/- mouse embryo fibroblasts. *Oncogene* **13**, 739-748 (1996).
704 38. Hoare, M. *et al.* NOTCH1 mediates a switch between two distinct secretomes during senescence.
705 *Nat Cell Biol* **18**, 979-992 (2016).
706 39. Innes, A.J. & Gil, J. IMR90 ER:RAS: A Cell Model of Oncogene-Induced Senescence. *Methods Mol*
707 *Biol* **1896**, 83-92 (2019).
708 40. Woods, D. *et al.* Raf-induced proliferation or cell cycle arrest is determined by the level of Raf
709 activity with arrest mediated by p21Cip1. *Mol Cell Biol* **17**, 5598-5611 (1997).
710 41. Hutter, E. *et al.* Senescence-associated changes in respiration and oxidative phosphorylation in
711 primary human fibroblasts. *Biochem J* **380**, 919-928 (2004).
712 42. Zhang, J. & Zhang, Q. Using Seahorse Machine to Measure OCR and ECAR in Cancer Cells. *Methods*
713 *Mol Biol* **1928**, 353-363 (2019).
714 43. Vizioli, M.G. *et al.* Mitochondria-to-nucleus retrograde signaling drives formation of cytoplasmic
715 chromatin and inflammation in senescence. *Genes & development* **34**, 428-445 (2020).

716 44. Velarde, M.C., Flynn, J.M., Day, N.U., Melov, S. & Campisi, J. Mitochondrial oxidative stress caused
717 by Sod2 deficiency promotes cellular senescence and aging phenotypes in the skin. *Aging (Albany*
718 *NY)* **4**, 3-12 (2012).
719 45. Macip, S. *et al.* Inhibition of p21-mediated ROS accumulation can rescue p21-induced senescence.
720 *EMBO J* **21**, 2180-2188 (2002).
721 46. Staal, F.J., Roederer, M., Herzenberg, L.A. & Herzenberg, L.A. Intracellular thiols regulate activation
722 of nuclear factor kappa B and transcription of human immunodeficiency virus. *Proc Natl Acad Sci U*
723 *S A* **87**, 9943-9947 (1990).
724 47. Leucci, E. *et al.* Melanoma addiction to the long non-coding RNA SAMMSON. *Nature* **531**, 518-522
725 (2016).
726 48. Tu, Y.T. & Barrientos, A. The Human Mitochondrial DEAD-Box Protein DDX28 Resides in RNA
727 Granules and Functions in Mitoribosome Assembly. *Cell Rep* **10**, 854-864 (2015).
728 49. Sheu, K.F. & Blass, J.P. The alpha-ketoglutarate dehydrogenase complex. *Ann N Y Acad Sci* **893**, 61-
729 78 (1999).
730 50. Shen, N. *et al.* DLST-dependence dictates metabolic heterogeneity in TCA-cycle usage among triple-
731 negative breast cancer. *Commun Biol* **4**, 1289 (2021).
732 51. Qattan, A.T., Radulovic, M., Crawford, M. & Godovac-Zimmermann, J. Spatial distribution of cellular
733 function: the partitioning of proteins between mitochondria and the nucleus in MCF7 breast cancer
734 cells. *J Proteome Res* **11**, 6080-6101 (2012).
735 52. Wang, Y. *et al.* KAT2A coupled with the alpha-KGDH complex acts as a histone H3
736 succinyltransferase. *Nature* **552**, 273-277 (2017).
737 53. Szklarczyk, D. *et al.* STRING v11: protein-protein association networks with increased coverage,
738 supporting functional discovery in genome-wide experimental datasets. *Nucleic Acids Res* **47**, D607-
739 D613 (2019).
740 54. Alvarez-Abril, B., Garcia-Martinez, E. & Galluzzi, L. Platinum-based chemotherapy inflames the
741 ovarian carcinoma microenvironment through cellular senescence. *Oncoimmunology* **11**, 2052411
742 (2022).
743 55. Murphy, M.P. How mitochondria produce reactive oxygen species. *Biochem J* **417**, 1-13 (2009).
744 56. Hamanaka, R.B. & Chandel, N.S. Mitochondrial reactive oxygen species regulate cellular signaling
745 and dictate biological outcomes. *Trends Biochem Sci* **35**, 505-513 (2010).
746 57. Davalli, P., Mitic, T., Caporali, A., Lauriola, A. & D'Arca, D. ROS, Cell Senescence, and Novel
747 Molecular Mechanisms in Aging and Age-Related Diseases. *Oxid Med Cell Longev* **2016**, 3565127
748 (2016).
749 58. Wei, Z. *et al.* CUL4B impedes stress-induced cellular senescence by dampening a p53-reactive
750 oxygen species positive feedback loop. *Free Radic Biol Med* **79**, 1-13 (2015).
751 59. Martinez-Reyes, I. & Chandel, N.S. Mitochondrial TCA cycle metabolites control physiology and
752 disease. *Nat Commun* **11**, 102 (2020).
753 60. Hansen, G.E. & Gibson, G.E. The alpha-Ketoglutarate Dehydrogenase Complex as a Hub of Plasticity
754 in Neurodegeneration and Regeneration. *Int J Mol Sci* **23** (2022).
755 61. Tretter, L. & Adam-Vizi, V. Inhibition of Krebs cycle enzymes by hydrogen peroxide: A key role of
756 [alpha]-ketoglutarate dehydrogenase in limiting NADH production under oxidative stress. *J*
757 *Neurosci* **20**, 8972-8979 (2000).
758 62. Sutendra, G. *et al.* A nuclear pyruvate dehydrogenase complex is important for the generation of
759 acetyl-CoA and histone acetylation. *Cell* **158**, 84-97 (2014).
760 63. Kafkia, E. *et al.* Operation of a TCA cycle subnetwork in the mammalian nucleus. *Sci Adv* **8**,
761 eabq5206 (2022).
762 64. Li, W. *et al.* Nuclear localization of mitochondrial TCA cycle enzymes modulates pluripotency via
763 histone acetylation. *Nat Commun* **13**, 7414 (2022).
764 65. Chen, J. *et al.* Compartmentalized activities of the pyruvate dehydrogenase complex sustain
765 lipogenesis in prostate cancer. *Nat Genet* **50**, 219-228 (2018).
766 66. Mellid, S. *et al.* DLST mutations in pheochromocytoma and paraganglioma cause proteome
767 hyposuccinylation and metabolic remodeling. *Cancer Commun (Lond)* (2023).

768 67. Ewald, J.A., Desotelle, J.A., Wilding, G. & Jarrard, D.F. Therapy-induced senescence in cancer. *J Natl*
769 *Cancer Inst* **102**, 1536-1546 (2010).
770 68. Pardella, E. *et al.* Therapy-Induced Stromal Senescence Promoting Aggressiveness of Prostate and
771 Ovarian Cancer. *Cells* **11** (2022).
772 69. Pranzini, E., Pardella, E., Paoli, P., Fendt, S.M. & Taddei, M.L. Metabolic Reprogramming in
773 Anticancer Drug Resistance: A Focus on Amino Acids. *Trends Cancer* **7**, 682-699 (2021).
774 70. Tan, Y. *et al.* Metabolic reprogramming from glycolysis to fatty acid uptake and beta-oxidation in
775 platinum-resistant cancer cells. *Nat Commun* **13**, 4554 (2022).
776 71. Jiang, P., Du, W., Mancuso, A., Wellen, K.E. & Yang, X. Reciprocal regulation of p53 and malic
777 enzymes modulates metabolism and senescence. *Nature* **493**, 689-693 (2013).
778 72. Castello, A. *et al.* Comprehensive Identification of RNA-Binding Proteins by RNA Interactome
779 Capture. *Methods Mol Biol* **1358**, 131-139 (2016).
780 73. Zhang, H. *et al.* LncRNA NEAT1 controls the lineage fates of BMSCs during skeletal aging by
781 impairing mitochondrial function and pluripotency maintenance. *Cell Death Differ* **29**, 351-365
782 (2022).
783 74. Vendramin, R., Marine, J.C. & Leucci, E. Non-coding RNAs: the dark side of nuclear-mitochondrial
784 communication. *EMBO J* **36**, 1123-1133 (2017).
785 75. Dieterle, F., Ross, A., Schlotterbeck, G. & Senn, H. Probabilistic quotient normalization as robust
786 method to account for dilution of complex biological mixtures. Application in 1H NMR
787 metabonomics. *Anal Chem* **78**, 4281-4290 (2006).
788 76. Veselkov, K.A. *et al.* Optimized preprocessing of ultra-performance liquid chromatography/mass
789 spectrometry urinary metabolic profiles for improved information recovery. *Anal Chem* **83**, 5864-
790 5872 (2011).
791 77. Athie, A. *et al.* Analysis of copy number alterations reveals the lncRNA ALAL-1 as a regulator of lung
792 cancer immune evasion. *J Cell Biol* **219** (2020).
793 78. Marin-Bejar, O. *et al.* The human lncRNA LINC-PINT inhibits tumor cell invasion through a highly
794 conserved sequence element. *Genome Biol* **18**, 202 (2017).
795 79. Liao, Y., Smyth, G.K. & Shi, W. featureCounts: an efficient general purpose program for assigning
796 sequence reads to genomic features. *Bioinformatics* **30**, 923-930 (2014).
797 80. Langmead, B. & Salzberg, S.L. Fast gapped-read alignment with Bowtie 2. *Nat Methods* **9**, 357-359
798 (2012).
799 81. Liberzon, A. *et al.* The Molecular Signatures Database (MSigDB) hallmark gene set collection. *Cell*
800 *Syst* **1**, 417-425 (2015).
801 82. Edgar, R., Domrachev, M. & Lash, A.E. Gene Expression Omnibus: NCBI gene expression and
802 hybridization array data repository. *Nucleic Acids Res* **30**, 207-210 (2002).
803 83. Perez-Riverol, Y. *et al.* The PRIDE database resources in 2022: a hub for mass spectrometry-based
804 proteomics evidences. *Nucleic Acids Res* **50**, D543-D552 (2022).

805

FIGURE LEGENDS

Figure 1. *sin-lncRNA* is a senescence-specific lncRNA transcriptionally induced by C/EBPβ. **A)** Schematic representation of normal fibroblasts undergoing OIS upon 4OHT-mediated activation of an oncogenic form of HRAS. **B)** Volcano plot depicting differential gene expression data (GSE61130) comparing IMR90 ER:RAS proliferating and senescent cells. Cut-off for significance $log_2FC>\pm1$; adj.Pvalue < 0.05. A selection of canonical senescence markers (in black) and lncRNAs (in red) is shown. **C)** RT-qPCR analysis of a set of lncRNA candidates upregulated upon 4OHT time course (3 or 6 days) in IMR90 ER:RAS cells; *RIPOR3-as1* was amplified with primer set#2 (see Suppl. Figure 2A for details) Data are presented as mean values ± s.d. n=3/4. **D)** Genomic snapshot of *sin-lncRNA* locus with RNA-seq tracks of untreated and 4OHT-treated IMR90 ER:RAS fibroblasts, as well as C/EBPβ ChIP-seq ENCODE data generated in IMR90 cells. **E)** RT-qPCR analysis of "young" (<14 passages), "old" (>30 passages) IMR90 fibroblasts and 4OHT-induced "OIS" IMR90 ER:RAS cells, shows that *sin-lncRNA* upregulation is maintained in replicative senescence, compared to p16 positive control. (n=2) **F)** Western blot analysis of control and C/EBPβ-depleted senescent IMR90 ER:RAS cells. Proliferating fibroblasts were used as further control. **G)** RT-qPCR analysis of *sin-lncRNA*, as well as a set of C/EBPβ-target genes in control and C/EBPβ-depleted senescent IMR90 ER:RAS cells. Data are represented as mean values ± s.d. (n=2) **H)** ChIP-qPCR analysis of C/EBPβ in proliferating and senescent IMR90 ER:RAS cells upon 6 days of 4OHT treatment. IgG IP was used as IP control; C/EBPβ peaks at *sin-lncRNA* locus are labeled according to their distance from *sin-lncRNA* TSS; regions located in *DDX11*, *GAPDH* and *HPRT* promoters served as negative controls, *IL6* and *IL8* promoter regions as positive controls (n=2).

Figure 2. *sin-lncRNA* depletion reinforces the senescent phenotype. **A)** RT-qPCR analysis of control and *sin-lncRNA* depleted IMR90 ER:RAS cells after 3 days of senescence induction. Primer sets #1 was used to amplify *sin-lncRNA* (see Suppl. Table4). Proliferating control cells were used as further control. Values were normalized to senescent control cells. **B)** Crystal violet assay and **C)** BrdU analysis assessing cell growth of control and *sin-lncRNA* depleted IMR90 ER:RAS fibroblasts after 5 days of senescence induction.

D) β-galactosidase analysis of control and *sin-lncRNA* depleted IMR90 cells induced to senescence for 8 days. **E)** Western blot analysis of control and *sin-lncRNA* depleted IMR90 cells treated with 4OHT for 5 days. **F)** RT-qPCR analysis of TIG3 ΔBRAF cell clones infected with *sin-lncRNA* sgRNA or an empty plasmid. **G)** BrdU (left) and β-galactosidase (right) assays of control or *sin-lncRNA* sgRNA TIG3 ΔBRAFclones. **H)** RT-qPCR and **I)** BrdU analysis of IMR90 ER:RAS cells transiently transfected with empty or *sin-lncRNA* construct upon OIS.

Figure 3. *sin-lncRNA* KD alters oxidative stress response and metabolic pathways in senescent cells. **A)** Volcano plot depicting differentially expressed genes comparing *sin-lncRNA* KD vs control IMR90 ER:RAS senescent cells. Upregulated genes (adj.Pvalue < 0.01; log2FC>1) are labeled in red, downregulated genes (adj.Pvalue < 0.01; log2FC<-1) in blue. **B)** Hallmark Gene Set Enrichment Analysis (GSEA) reporting the most enriched pathways associated to the genes differentially expressed (DE) upon *sin-lncRNA* depletion (threshold: adj.Pvalue<1e-4). **C)** Heatmap highlighting expression changes across RNA-seq replicates of genes belonging to OXIDATIVE_PHOSPHORILATION GSEA pathway. **D)** Quantification of different parameters of the oxygen consumption rates (OCR) in control and *sin-lncRNA* depleted (siRNA#1/3) IMR90 ER:RAS, assessed through Seahorse technology. The graph represents the mean ± s.d. (n=4). Two tailed student's *t*-test, **p*<0.05. A representative OCR curve for each cell line is included in (Supplementary Fig. 4). **E)** Basal extracellular acidification rate (ECAR) levels measured using the seahorse technology in control or *sin-lncRNA* depleted IMR90 ER:RAS senescent cells. Values were normalized to the total amount of protein per condition. **F)** Fluorometric analysis measuring the amount of the fluorescent oxidized probe 2′,7′-dichlorofluorescein (DCF), as indicative of ROS/NOS intracellular levels in control and *sin-lncRNA* depleted IMR90 ER:RAS fibroblasts induced to senescence for 5 days. Proliferating control cells were used as further control. **G)** Absorbance levels of crystal violet solution measured at 560 nm from vehicle or N-acetyl-L-cisteine (NAC)-treated IMR90 ER:RAS fibroblasts transfected with siRNA control (CTRL) or against *sin-lncRNA* (sin#1/3) and induced to senescence for 5 days. The graph represents the mean ± s.d. (n=3). Two tailed student's *t*-test, **p*<0.05.

Figure 4. *sin-lncRNA* interacts with DLST and affects metabolism of senescent cells by regulating DLST localization. **A)** RNA-FISH based on locked nucleic acid (LNA) technology on fixed IMR90 ER:RAS cells depleted or not of *sin-lncRNA* (siRNA_sin-lncRNA#1/3) and treated for 5 days with 4OHT. Two different LNAs were used. Incubation without LNA probe ("No_probe") was used as control. **B)** List of top candidate proteins identified by mass spectrometry after pulldown with in vitro biotinylated *sin-lncRNA*. **C)** Schematic representation of the TCA cycle that takes place in the mitochondria. DLST enzyme is highlighted in red. **D)** RNA immunoprecipitation analysis monitoring DLST binding to *sin-lncRNA, MALAT1* and *GAPDH* RNA in control and *sin-lncRNA* depleted (siRNA#1/3) senescent IMR90 ER:RAS, using anti-DLST antibody or IgG as a negative control. The graph represents the mean ± s.d. (n=2). **E)** *Left*, representative β-galactosidase images of untreated control cells and control, *sin-lncRNA* depleted or DLST-depleted IMR90 cells induced to senescence for 5 days. Scale bar: 50 µm. *Right*, quantification of the percentage of β-galactosidase positive cells in each condition normalized to control untreated cells set as 1. The graph represents the mean ± s.d. (n=4). Two tailed student's *t*-test, $**p<0.01$. **F)** Absorbance levels of crystal violet solution measured at 560 nm in the conditions described in E. The graph represents the mean ± s.d. (n=4). Two tailed student's *t*-test, $*p<0.05$. **G)** Lactate levels measured from the supernatant of IMR90 ER:RAS fibroblasts transfected with the indicated siRNA and induced with 4OHT for 3 or 6 days. The graph represents the mean ± s.d. (n=3). Two tailed student's *t*-test, $*p<0.05$; $**p<0.01$; $***p<0.001$. **H)** *Left*, western blot analysis of DLST cellular fractionation in control and *sin-lncRNA* depleted (siRNA#1/3) senescent IMR90 ER:RAS. GAPDH and H3 were used as cytoplasmic and nuclear controls respectively. *Right*, percentage of nuclear and cytoplasmic distribution of DLST normalized to GAPDH (cyto) or H3 (nucl). The graph represents the mean ± s.d. (n=3). Two tailed student's *t*-test, $**p<0.01$.

Figure 5. *sin-lncRNA* regulates OXPHOS in ovarian cancer cells. **A)** Representative β-galactosidase images of untreated COV362 cells (upper panel) or treated for 10 days with µM cisplatin. Scale bar: 50 µm. Numbers represent the mean ± s.d. (n=3). **B)** RT-qPCR analysis of senescence markers genes in cisplatin treated COV362 for 10 days compared to untreated controls (set as 1). **C)** RT-qPCR analysis of *sin-lncRNA* in the cells described in B. The graph represents the mean ± s.d. (n=4). One sample *t*-test, $**p<0.01$. **D)**

Western blot analysis of C/EBPβ protein levels in the cells described in B. Numbers represent the mean ± s.d. (n=3). **E)** RT-qPCR analysis of OXPHOS GSEA pathway genes in control and *sin-lncRNA* depleted (siRNA#1/3) COV362 senescent cells treated with cisplatin for 10 days. **F)** Quantification of different parameters of the oxygen consumption rates (OCR) in proliferating cells compared to control or *sin-lncRNA* depleted (siRNA#1/3) senescent COV362 cells, assessed through Seahorse technology. The graph represents the mean ± s.d. (n=4). Two tailed student's *t*-test, $*p<0.05$; $**p<0.01$. **G)** Basal extracellular acidification rate (ECAR) levels measured using the seahorse technology in the same conditions as in F. The graph represents the mean ± s.d. (n=4). Two tailed student's *t*-test, $*p<0.05$. **H)** Absorbance levels of crystal violet solution measured at 560 nm in proliferating or senescent COV362 cells transfected with control, *sin-lncRNA* or DLST siRNA treated for 10 days with 10 μM cisplatin.

SUPPLEMENTARY FIGURE LEGENDS

Suppl. Figure 1. A) Change in proliferation rate comparing proliferating and senescent IMR90 ER:RAS fibroblasts, as measured by BrdU assay. **B)** Representative images of crystal violet staining in untreated or 4-OHT treated cells for 5 days. **C)** Representative images of the β-galactosidase staining in untreated cells or treated with 4-OHT for 8 days. **D)** qRT-PCR analysis of CXCL1 and IL1A upregulation in untreated or 4-OHT treated cells for 5 days. **E)** Western blot analysis of senescence markers p53, p21 and p16 in untreated or 4-OHT treated cells for 5 days. **F)** DAPI staining and **G)** Immunostaining images of gH2A.X, H3K96m3 and DAPI of untreated or 4OHT treated IMR90 ER:RAS for 5 days. **H)** Pie chart representation of the number of biotype distribution of transcripts deregulated during OIS (log_2-fold change >±1, adj.Pvalue <0.05). **I)** Heat map showing relative expression of senescence markers and lncRNAs deregulated in IMR90 ER:RAS untreated or treated with 4-OHT for 8 days.

Suppl. Figure 2. A) Genomic snapshot of *sin-lncRNA* (RIPOR3-as) locus PolyA sites annotated by Genecode v19 are indicated as well as the position of qPCR primers used to amplify the different isoforms. Bottom panel, qRT-PCR analysis of the different annotated isoforms of *sin-lncRNA* (RIPOR3-as) using different set of primers (set1-3) in a time course of 3 and 6 days of senescence induction in IMR90 ER:RAS cells. **B)** qRT-PCR analysis of protein-coding gene RIPOR3 in a time course of 3 and 6 days of senescence induction in IMR90 ER:RAS cells. **C)** CPAT software was interrogated to determine the coding probability of *sin-lncRNA*. GAPDH mRNA and MALAT1 lncRNA were used as coding and noncoding references, respectively. **D)** Number of copies per cell of *sin-lncRNA* in control untreated cells and in 4-OHT-treated cells measured by qRT–PCR using dilutions of a pcDNA3.1-*sin-lncRNA* plasmid as standard curve. **E)** RT-qPCR analysis showing *sin-lncRNA* upregulation upon treatment with γ-irradiation at 5Gy in IMR90 fibroblasts. *p16* and *IL6* levels served as positive controls. **F)** Western blot analysis of C/EBPβ of IMR90 ER:RAS cells treated or not with 4OHT for 3 or 6 days. **G)** qRT-PCR analysis of the levels of C/EBPβ in control and C/EBPβ-depleted senescent IMR90 ER:RAS cells

Suppl. Figure 3. A) RT-qPCR analysis of control and *sin-lncRNA* depleted IMR90 ER:RAS cells after 3 days of senescence induction. Proliferating control cells were used as further control. Primer sets #2 (Suppl. Figure 2A) were used to amplify *sin-lncRNA*. Values were normalized to senescent control cells. **B)** BrdU analysis measuring the proliferation of control and *sin-lncRNA* depleted IMR90 ER:RAS cells after 5 days of senescence induction. Proliferating control cells were used as further control. Values were normalized to senescent control cells. **C)** RT-qPCR analysis of control and *sin-lncRNA* depleted TIG3-hTERT:BRAF cells after 3 days of senescence induction. Proliferating control cells were used as further control. Primer sets #3 (Suppl. Figure 2A) were used to amplify *sin-lncRNA*. Values were normalized to senescent control cells. **D)** BrdU staining and **E)** relative growth measured by crystal violet at 570nm absorbance of control and *sin-lncRNA* depleted TIG3-hTERT:BRAF cells after 5 days of senescence induction. Proliferating control cells were used as further control. Values were normalized to senescent control cells. **F)** Schematic representation of the CIRSPR/Cas9 strategy applied to remove *sin-lncRNA* genetic loci. sgRNAs guiding Cas9 protein are indicated (sgRNA_up and sgRNA_dw), as well as inner and outer primer couples to screen engineered cell clones (fwd/rev_in and fwd/rev_out, respectively) **G)** Gel images showing PCR products obtained using outer (left) or inner primer sets (right) to amplify the genome of TIG3 BRAF single cell clones after infection with the lentiCRISPR carrying *sin-lncRNA* sgRNAs and selection (clone#n). TIG3 BRAF fibroblasts infected with empty lentiviral vector (Empty) or infected with vector carrying *sin-lncRNA* sgRNAs but without single cell separation and puro selection (CRISPR_unsorted) were used as control. **H)** Representation of *sin-lncRNA* isoform amplified from cDNA samples and cloned in pcDNA3.1 plasmid. **I)** BrdU analysis measuring the proliferation of IMR90 ER:RAS cells transiently transfected with empty or *sin-lncRNA* expression vector and 4OHT-treated for 5 days. Proliferating cells transfected with empty vector were used as further control.

Suppl. Figure 4. A) RT-qPCR analysis of the indicated transcripts in control and *sin-lncRNA* depleted IMR90 ER:RAS cells after 5 days of senescence induction. Proliferating control cells were used as further control. Values were normalized to senescent control cells. **B)** Gene Set Enrichment Analysis (GSEA) for genes belonging to epithelial to mesenchymal transition and E2F-targets pathways. **C)** Oxygen

Consumption Rate (OCR) measurements were obtained over time (min) using the seahorse technology from control or *sin-lncRNA* depleted IMR90 ER:RAS senescent cells. Values were normalized to the total amount of protein per condition. The graph shows a representative experiment. **D)** Percentage of β-galactosidase positive cells in control or *sin-lncRNA* depleted IMR90 ER:RAS senescent cells treated with 5mM vehicle (DMSO) or N-acetyl-L-cisteine (NAC). **E)** Percentage of nuclear and cytoplasmic RNA levels of *sin-lncRNA* measured by qRT–PCR after cell fractionation with two different set of primers (set#1 and set#2) in untreated or 4OHT-induced senescent cells. **F)** Western blot analysis of the immunoprecipitated DLST using anti-DLST antibody or IgG as a negative control. GAPDH was used as control. (n=2) **G)** Western blot analysis of control IMR90 ER:RAS cells or cells transfected with siRNAs against *sin-lncRNA* or DLST. Proliferating control cells were used as further control. **H)** RT-qPCR analysis in control, DLST or *sin-lncRNA* depleted IMR90 ER:RAS cells after 3 days of senescence induction. Values were normalized to senescent control cells. Data are presented as mean ± s.d (n=4). Two tailed student's *t*-test, $*p<0.05$; $**p<0.01$. **I)** Western blot analysis of DLST protein levels in untreated IMR90 ER:RAS cells or treated for 3 or 6 days. GAPDH was used as a loading control.

Suppl. Figure 5. A) *Sin-lncRNA* expression (as FPKM + pseudocount value) across tumor samples from the TCGA database. **B)** Protein-Protein Interaction network (*p-value*$<1.0e^{-16}$) by STRING analysis of genes inversely correlated with *sin-lncRNA* (92 genes; R< -0.5). **C)** Gene Ontology (GO) pathways associated with the inversely correlated genes.

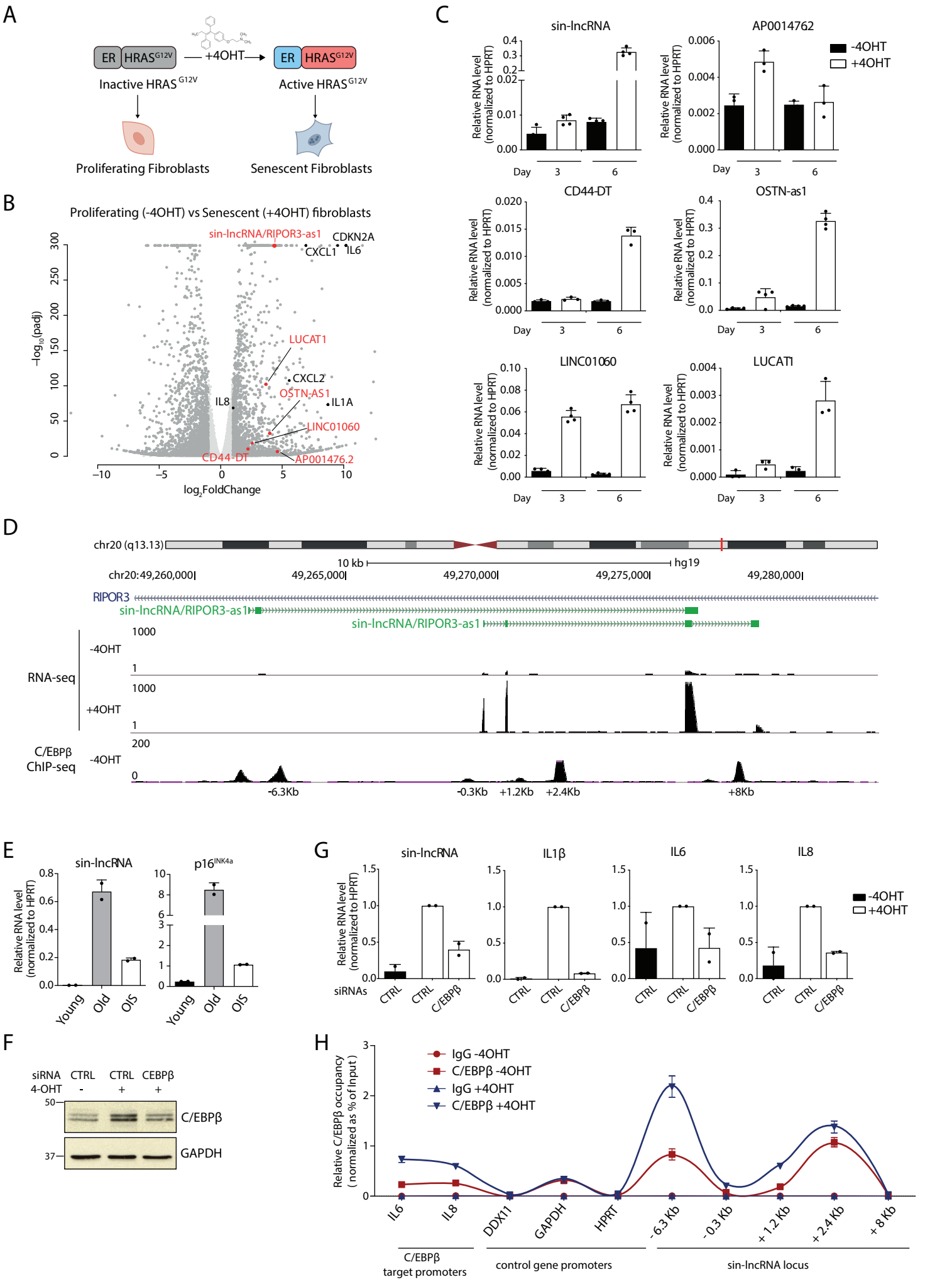
A
ER HRAS G12V
+4OHT
ER HRAS G12V
Inactive HRAS G12V
Active HRAS G12V
Proliferating Fibroblasts
Senescent Fibroblasts
B
Proliferating (-4OHT) vs Senescent (+4OHT) fibroblasts
sin-lncRNA/RIPOR3-as1
CDKN2A
CXCL1
IL6
LUCAT1
CXCL2
OSTN-AS1
IL8
IL1A
LINC01060
CD44-DT
AP001476.2
−log10(padj)
log2FoldChange
C
sin-lncRNA
AP0014762
CD44-DT
OSTN-as1
LINC01060
LUCAT1
Relative RNA level (normalized to HPRT)
Day
-4OHT
+4OHT
D
chr20 (q13.13)
10 kb
hg19
chr20:49,260,000
49,265,000
49,270,000
49,275,000
49,280,000
RIPOR3
sin-lncRNA/RIPOR3-as1
RNA-seq
-4OHT
+4OHT
C/EBPβ ChIP-seq
-6.3Kb
-0.3Kb
+1.2Kb
+2.4Kb
+8Kb
E
sin-lncRNA
p16INK4a
Young
Old
OIS
G
sin-lncRNA
IL1β
IL6
IL8
siRNAs
CTRL
C/EBPβ
F
siRNA
4-OHT
CTRL
CEBPβ
C/EBPβ
GAPDH
H
IgG -4OHT
C/EBPβ -4OHT
IgG +4OHT
C/EBPβ +4OHT
Relative C/EBPβ occupancy (normalized as % of Input)
IL6
IL8
DDX11
GAPDH
HPRT
- 6.3 Kb
- 0.3 Kb
+ 1.2 Kb
+ 2.4 Kb
+ 8 Kb
C/EBPβ target promoters
control gene promoters
sin-lncRNA locus

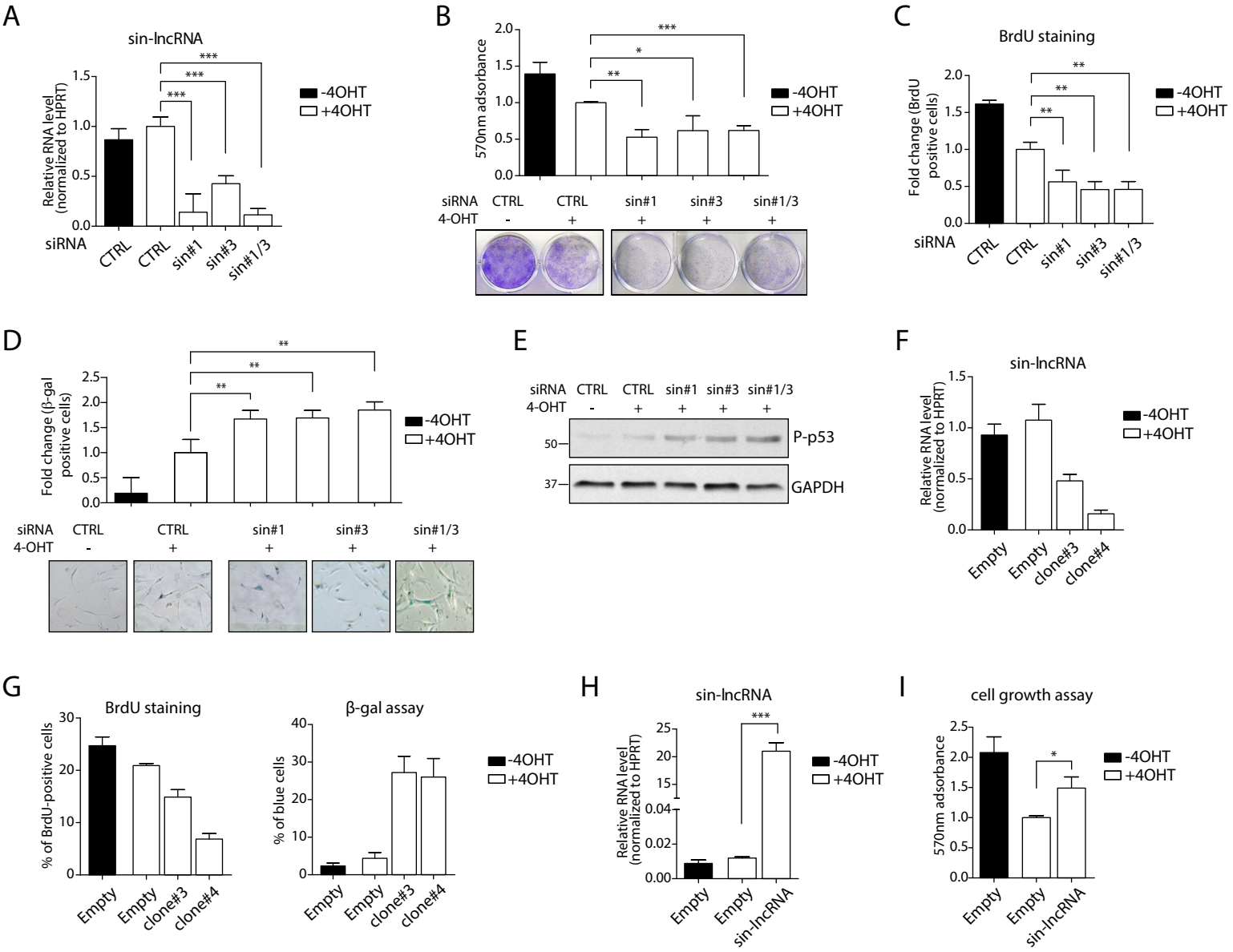
A
sin-lncRNA
Relative RNA level (normalized to HPRT)
-4OHT
+4OHT
siRNA
CTRL
CTRL
sin#1
sin#3
sin#1/3
B
570nm adsorbance
siRNA
4-OHT
C
BrdU staining
Fold change (BrdU positive cells)
D
Fold change (β-gal positive cells)
E
P-p53
GAPDH
F
sin-lncRNA
Empty
clone#3
clone#4
G
BrdU staining
% of BrdU-positive cells
β-gal assay
% of blue cells
H
sin-lncRNA
I
cell growth assay

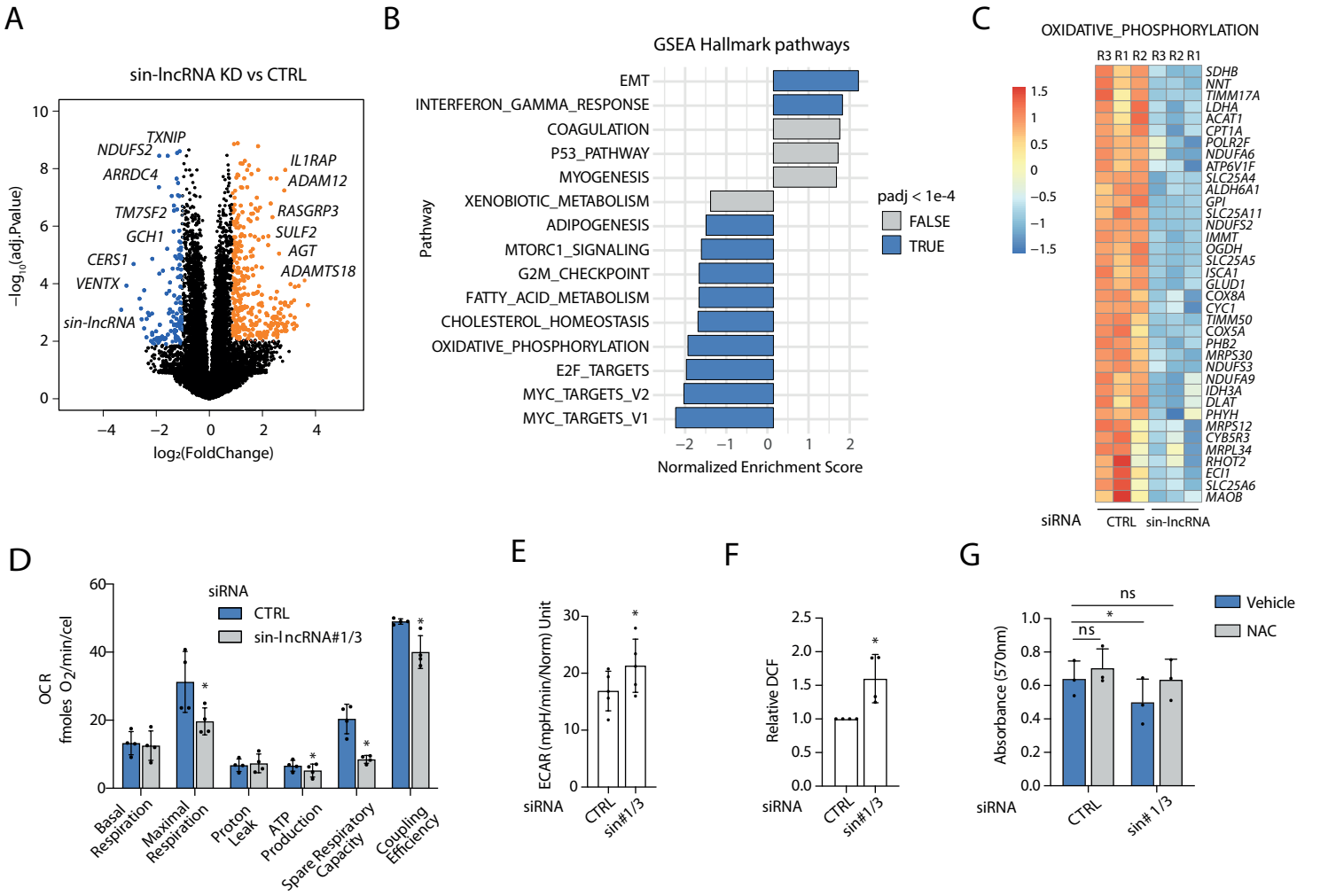
A
sin-lncRNA KD vs CTRL
TXNIP
NDUFS2
ARRDC4
TM7SF2
GCH1
CERS1
VENTX
sin-lncRNA
IL1RAP
ADAM12
RASGRP3
SULF2
AGT
ADAMTS18
−log10(adj.Pvalue)
log2(FoldChange)
B
GSEA Hallmark pathways
EMT
INTERFERON_GAMMA_RESPONSE
COAGULATION
P53_PATHWAY
MYOGENESIS
XENOBIOTIC_METABOLISM
ADIPOGENESIS
MTORC1_SIGNALING
G2M_CHECKPOINT
FATTY_ACID_METABOLISM
CHOLESTEROL_HOMEOSTASIS
OXIDATIVE_PHOSPHORYLATION
E2F_TARGETS
MYC_TARGETS_V2
MYC_TARGETS_V1
Pathway
padj < 1e-4
FALSE
TRUE
Normalized Enrichment Score
C
OXIDATIVE_PHOSPHORYLATION
R3 R1 R2 R3 R2 R1
SDHB
NNT
TIMM17A
LDHA
ACAT1
CPT1A
POLR2F
NDUFA6
ATP6V1F
SLC25A4
ALDH6A1
GPI
SLC25A11
NDUFS2
IMMT
OGDH
SLC25A5
ISCA1
GLUD1
COX8A
CYC1
TIMM50
COX5A
PHB2
MRPS30
NDUFS3
NDUFA9
IDH3A
DLAT
PHYH
MRPS12
CYB5R3
MRPL34
RHOT2
ECI1
SLC25A6
MAOB
siRNA
CTRL
sin-lncRNA
D
siRNA
CTRL
sin-lncRNA#1/3
OCR
fmoles O2/min/cel
Basal Respiration
Maximal Respiration
Proton Leak
ATP Production
Spare Respiratory Capacity
Coupling Efficiency
E
ECAR (mpH/min/Norm) Unit
siRNA
CTRL
sin#1/3
F
Relative DCF
siRNA
CTRL
sin#1/3
G
Vehicle
NAC
ns
Absorbance (570nm)
siRNA
CTRL
sin# 1/3

A

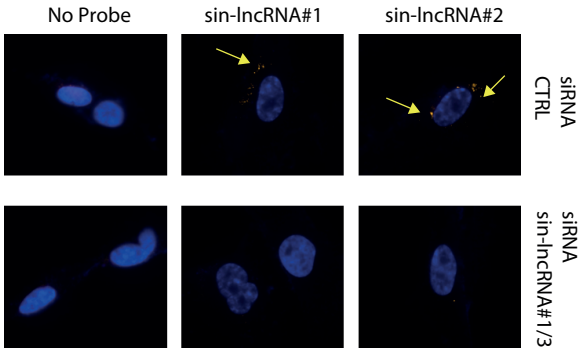

B

Gene	Unique	Total	MW (kDa)
DLST	5	5	48.72
DDX28	4	4	59.54
SEPT11	3	4	49.37
P4HA1	3	3	61.01
RAD23B	3	2	43.14
DAPK3	2	2	52.50
RMDN3	2	2	52.09
NKAPL	2	2	46.28
SNX18	2	2	68.85
VPS4A	2	2	48.87
ARCN1	2	2	57.17

C

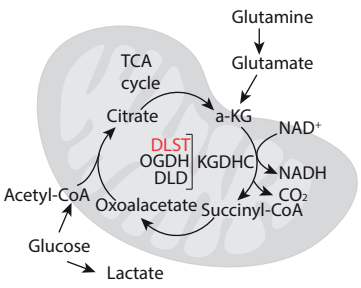

D

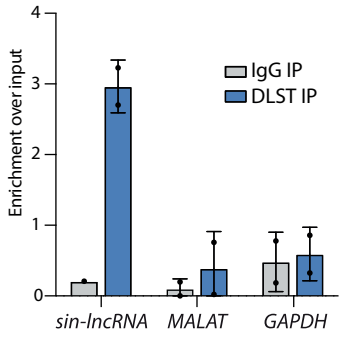

E

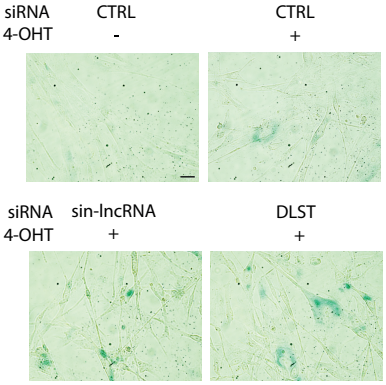

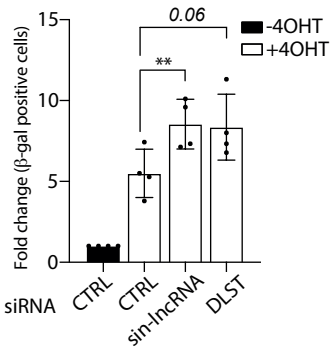

F

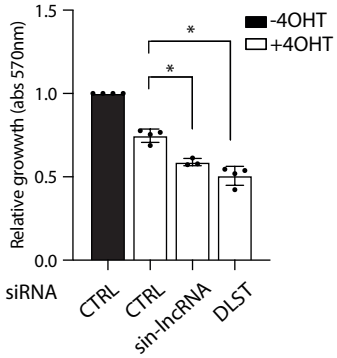

G

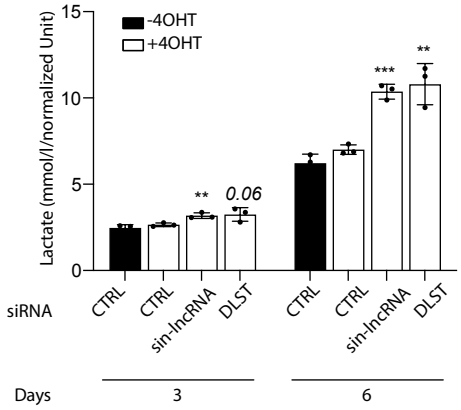

H

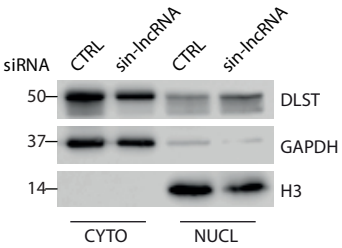

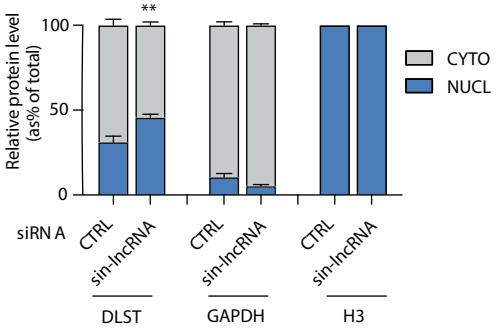

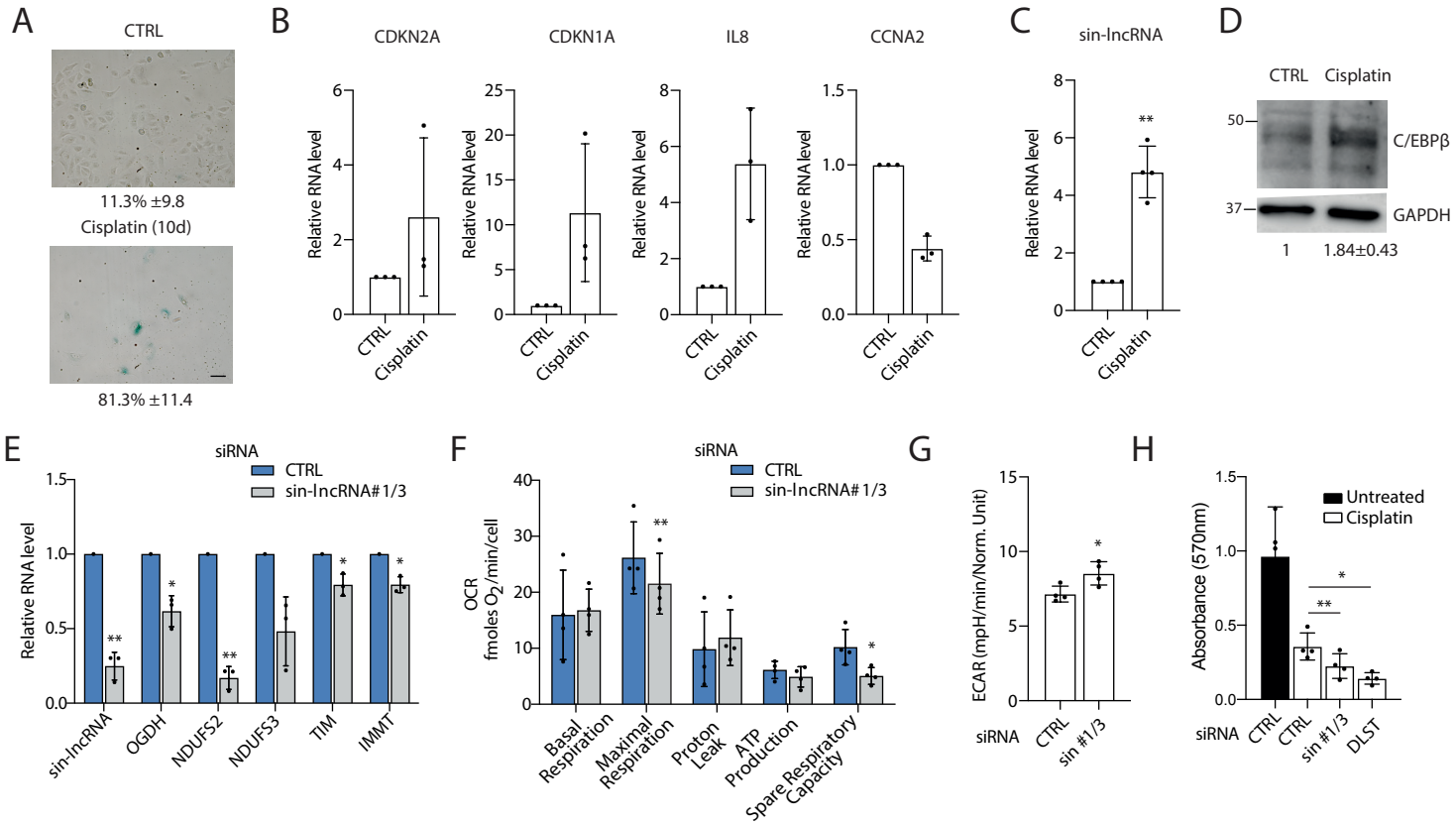
A
CTRL
11.3% ±9.8
Cisplatin (10d)
81.3% ±11.4
B
CDKN2A
CDKN1A
IL8
CCNA2
Relative RNA level
CTRL
Cisplatin
C
sin-lncRNA
D
CTRL
Cisplatin
C/EBPβ
GAPDH
1
1.84±0.43
E
siRNA
CTRL
sin-lncRNA#1/3
sin-lncRNA
OGDH
NDUFS2
NDUFS3
TIM
IMMT
F
OCR
fmoles O2/min/cell
Basal Respiration
Maximal Respiration
Proton Leak
ATP Production
Spare Respiratory Capacity
G
ECAR (mpH/min/Norm. Unit)
siRNA
CTRL
sin #1/3
H
Absorbance (570nm)
Untreated
Cisplatin
DLST

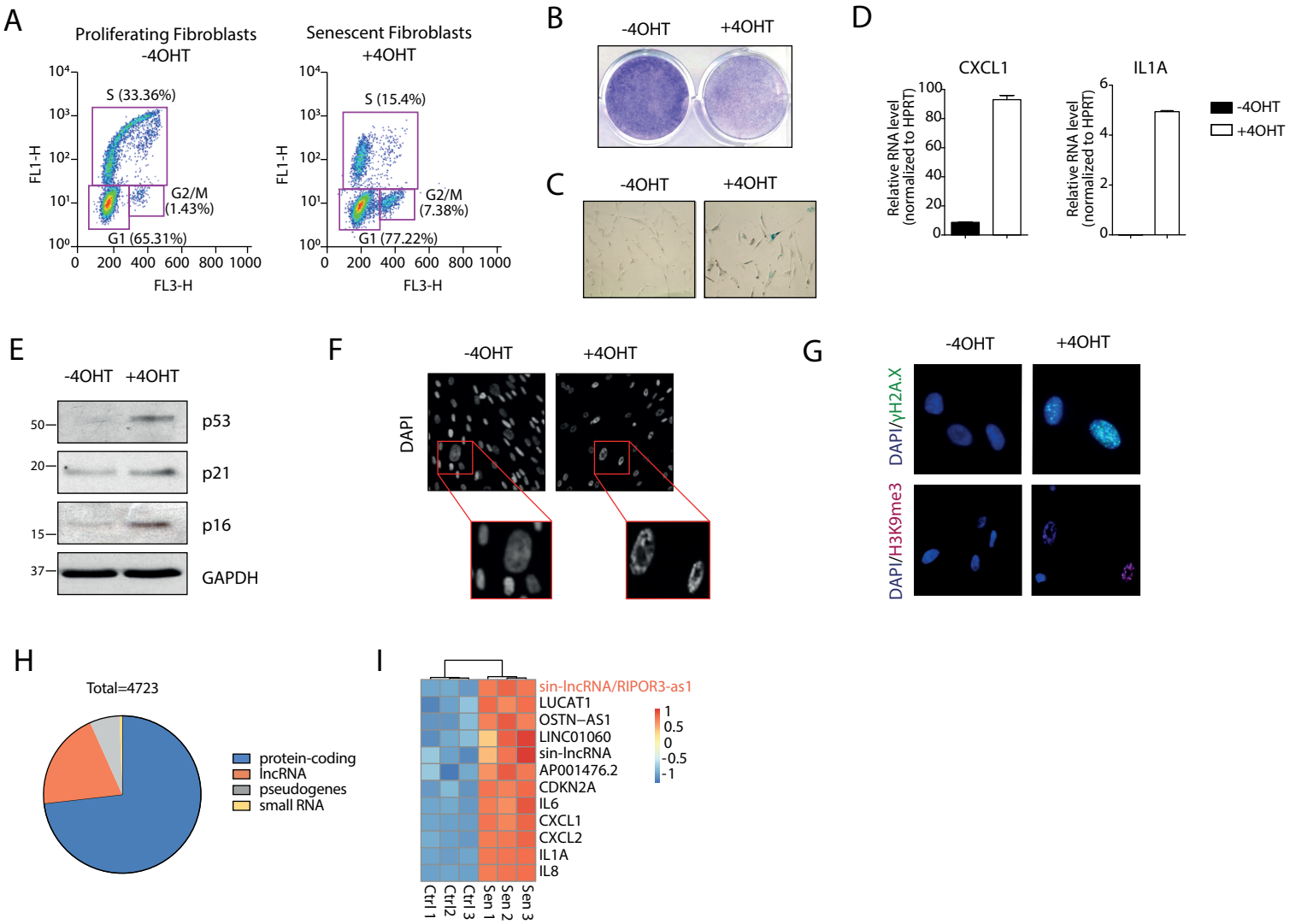
A
Proliferating Fibroblasts
-4OHT
Senescent Fibroblasts
+4OHT
S (33.36%)
G2/M (1.43%)
G1 (65.31%)
S (15.4%)
G2/M (7.38%)
G1 (77.22%)
FL1-H
FL3-H
B
-4OHT
+4OHT
C
-4OHT
+4OHT
D
CXCL1
IL1A
Relative RNA level (normalized to HPRT)
-4OHT
+4OHT
E
-4OHT
+4OHT
p53
p21
p16
GAPDH
F
-4OHT
+4OHT
DAPI
G
-4OHT
+4OHT
DAPI/γH2A.X
DAPI/H3K9me3
H
Total=4723
protein-coding
lncRNA
pseudogenes
small RNA
I
sin-lncRNA/RIPOR3-as1
LUCAT1
OSTN–AS1
LINC01060
sin-lncRNA
AP001476.2
CDKN2A
IL6
CXCL1
CXCL2
IL1A
IL8
Ctrl 1
Ctrl2
Ctrl 3
Sen 1
Sen 2
Sen 3

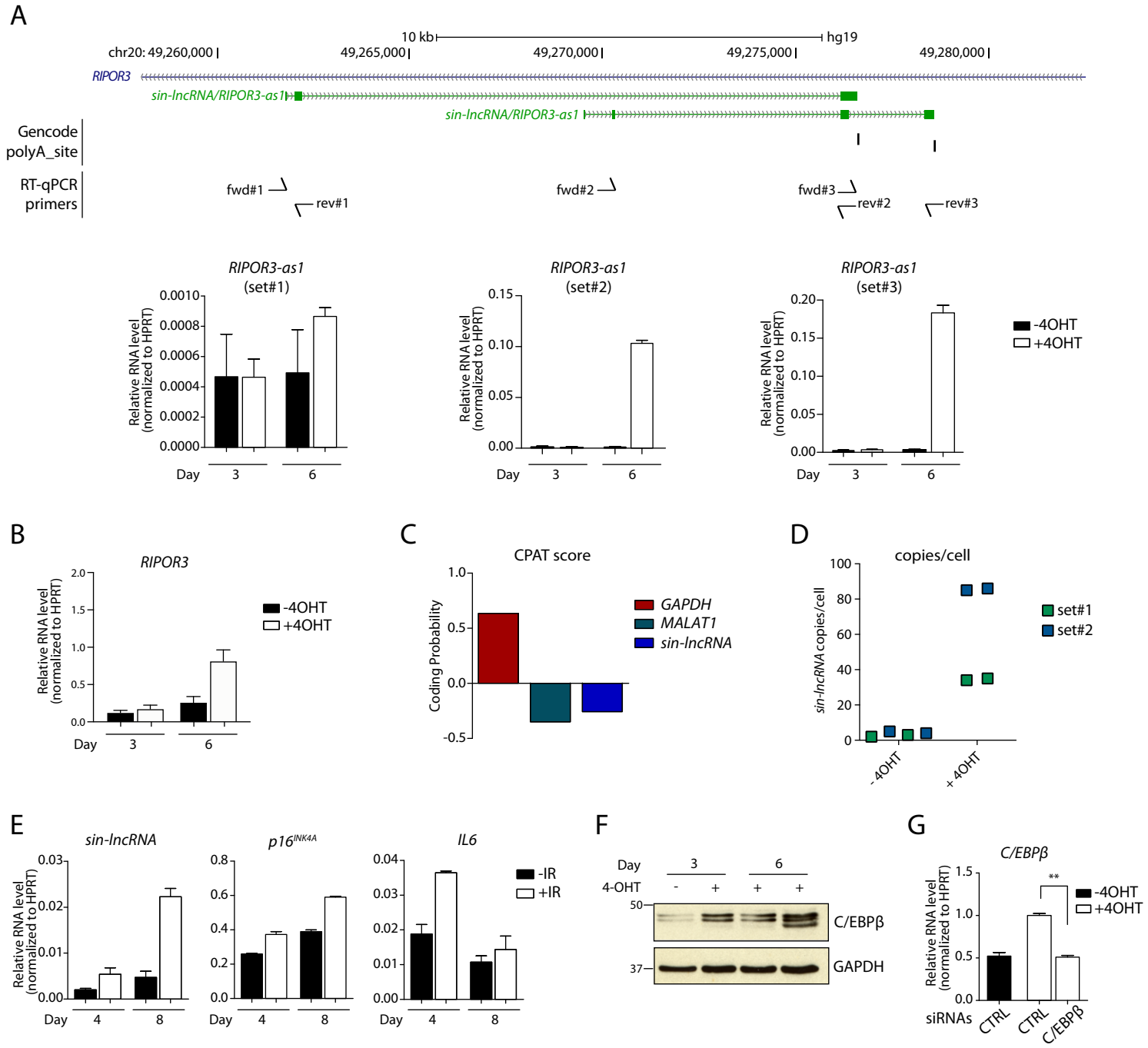
A
10 kb
hg19
chr20: 49,260,000
49,265,000
49,270,000
49,275,000
49,280,000
RIPOR3
sin-lncRNA/RIPOR3-as1
sin-lncRNA/RIPOR3-as1
Gencode polyA_site
RT-qPCR primers
fwd#1
rev#1
fwd#2
fwd#3
rev#2
rev#3
RIPOR3-as1 (set#1)
RIPOR3-as1 (set#2)
RIPOR3-as1 (set#3)
Relative RNA level (normalized to HPRT)
Day
-4OHT
+4OHT
B
RIPOR3
C
CPAT score
Coding Probability
GAPDH
MALAT1
sin-lncRNA
D
copies/cell
sin-lncRNA copies/cell
set#1
set#2
-4OHT
+4OHT
E
sin-lncRNA
p16INK4A
IL6
-IR
+IR
F
Day
4-OHT
C/EBPβ
GAPDH
G
C/EBPβ
siRNAs
CTRL
CTRL
C/EBPβ

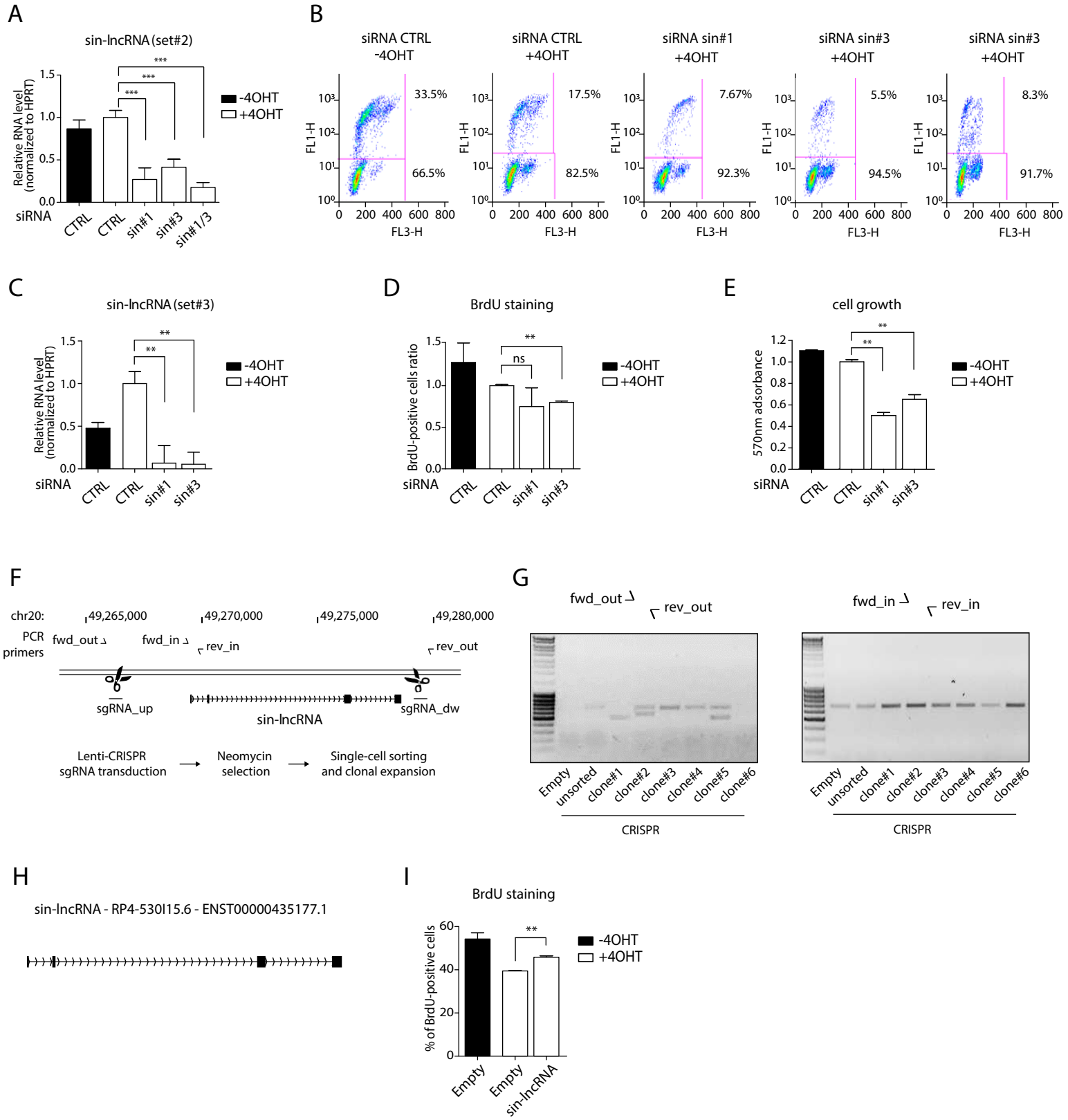
A
sin-lncRNA (set#2)
Relative RNA level (normalized to HPRT)
-4OHT
+4OHT
siRNA
CTRL
CTRL
sin#1
sin#3
sin#1/3
B
siRNA CTRL -4OHT
siRNA CTRL +4OHT
siRNA sin#1 +4OHT
siRNA sin#3 +4OHT
siRNA sin#3 +4OHT
FL1-H
FL3-H
33.5%
66.5%
17.5%
82.5%
7.67%
92.3%
5.5%
94.5%
8.3%
91.7%
C
sin-lncRNA (set#3)
D
BrdU staining
BrdU-positive cells ratio
ns
E
cell growth
570nm adsorbance
F
chr20:
49,265,000
49,270,000
49,275,000
49,280,000
PCR primers
fwd_out
fwd_in
rev_in
rev_out
sgRNA_up
sin-lncRNA
sgRNA_dw
Lenti-CRISPR sgRNA transduction
Neomycin selection
Single-cell sorting and clonal expansion
G
fwd_out
rev_out
fwd_in
rev_in
Empty
unsorted
clone#1
clone#2
clone#3
clone#4
clone#5
clone#6
CRISPR
H
sin-lncRNA - RP4-530I15.6 - ENST00000435177.1
I
BrdU staining
% of BrdU-positive cells
Empty
Empty
sin-lncRNA

A

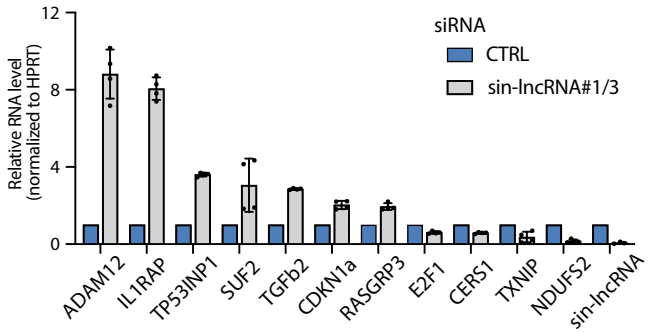

B

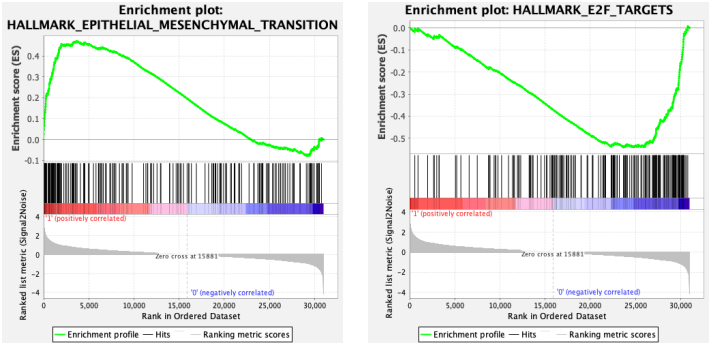

NES= 2.1
FDR < $1e^{-4}$

NES= -2.51
FDR < $1e^{-4}$

C

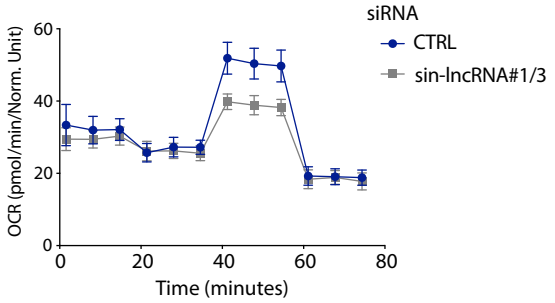

D

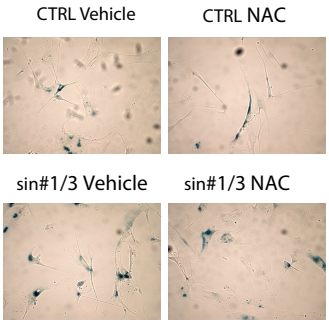

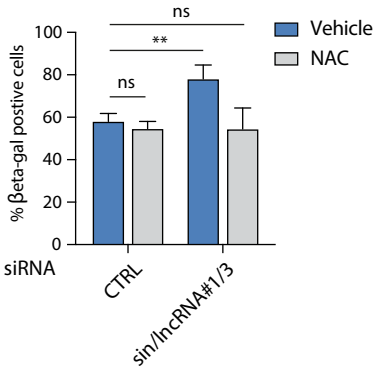

E

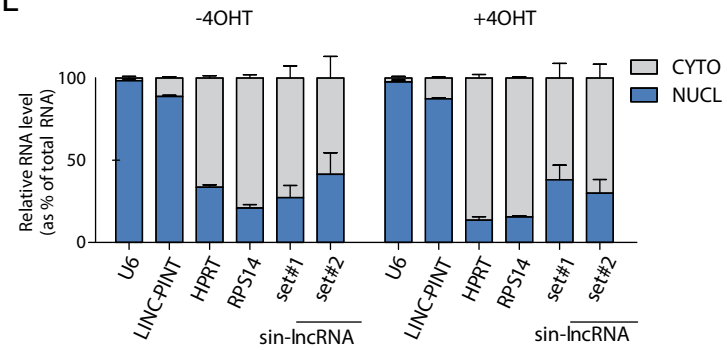

F

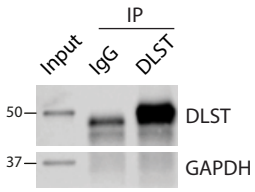

G

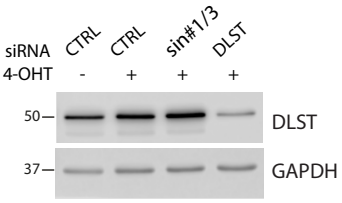

H

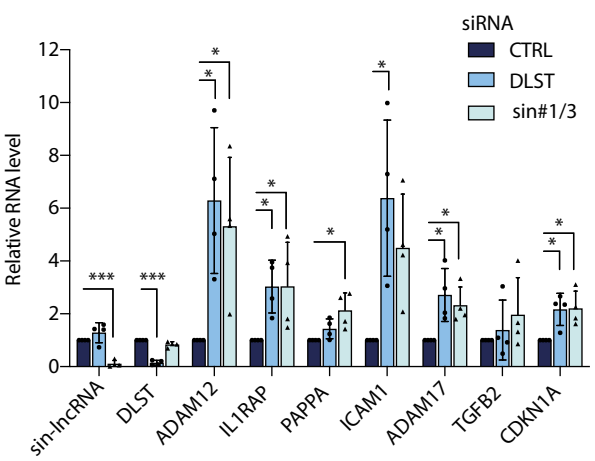

I

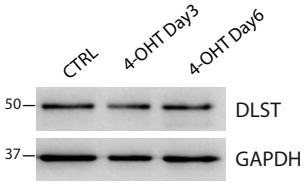

A

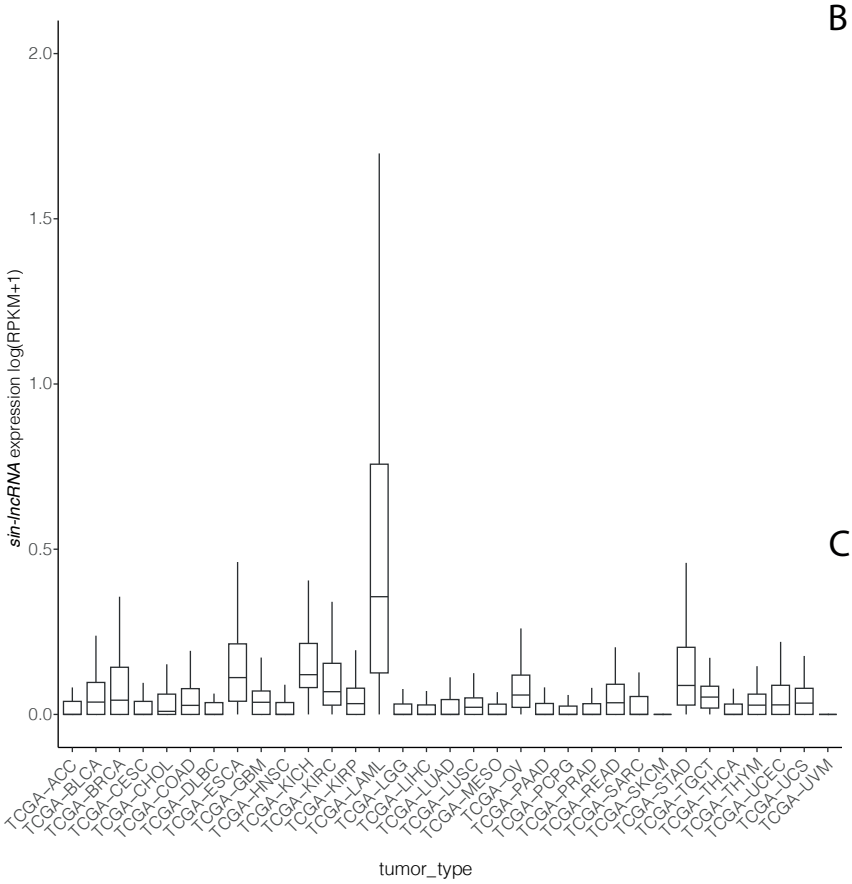

B

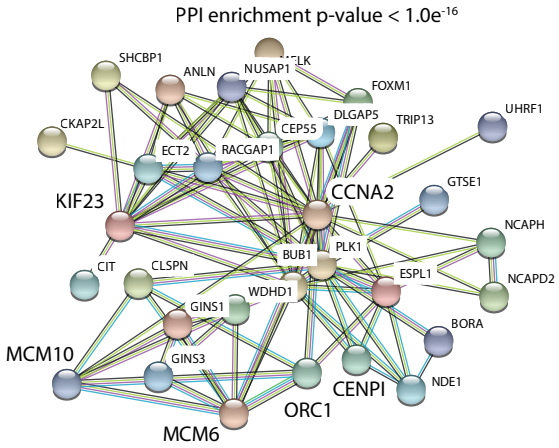

C

GO analysis - 92 inversely correlated genes (R< -0.5)

	ID	Name	p-value	FDR B&H
1	GO:0022402	cell cycle process	$6.52e^{-19}$	$1.63e^{-15}$
2	GO:0000278	mitotic cell cycle	$2.64e^{-16}$	$1.65e^{-13}$
3	GO:0051301	cell division	$6.14e^{-13}$	$3.07e^{-10}$